HHS Public Access

Author manuscript

Cell Rep. Author manuscript; available in PMC 2021 March 30.

Published in final edited form as:

Cell Rep. 2021 March 02; 34(9): 108777. doi:10.1016/j.celrep.2021.108777.

Optic nerve regeneration screen identifies multiple genes restricting adult neural repair

Jane A. Lindborg[1], **Nicholas M. Tran**[2], **Devon M. Chenette**[1], **Kristin DeLuca**[1], **Yram Foli**[1], **Ramakrishnan Kannan**[1], **Yuichi Sekine**[1], **Xingxing Wang**[1], **Marius Wollan**[1], **In-Jung Kim**[3], **Joshua R. Sanes**[2], **Stephen M. Strittmatter**[1,4,*]

[1]Cellular Neuroscience, Neurodegeneration, Repair, Departments of Neurology and of Neuroscience, Yale University School of Medicine, New Haven, CT 06536, USA

[2]Center for Brain Science and Department of Molecular and Cellular Biology, Harvard University, Cambridge, MA, USA

[3]Department of Ophthalmology and Visual Science, Yale University School of Medicine, New Haven, CT 06536, USA

[4]Lead contact

SUMMARY

Adult mammalian central nervous system (CNS) trauma interrupts neural networks and, because axonal regeneration is minimal, neurological deficits persist. Repair via axonal growth is limited by extracellular inhibitors and cell-autonomous factors. Based on results from a screen *in vitro*, we evaluate nearly 400 genes through a large-scale *in vivo* regeneration screen. Suppression of 40 genes using viral-driven short hairpin RNAs (shRNAs) promotes retinal ganglion cell (RGC) axon regeneration after optic nerve crush (ONC), and most are validated by separate CRISPR-Cas9 editing experiments. Expression of these axon-regeneration-suppressing genes is not significantly altered by axotomy. Among regeneration-limiting genes, loss of the interleukin 22 (IL-22) cytokine allows an early, yet transient, inflammatory response in the retina after injury. Reduced IL-22 drives concurrent activation of signal transducer and activator of transcription 3 (Stat3) and dual leucine zipper kinase (DLK) pathways and upregulation of multiple neuron-intrinsic regeneration-associated genes (RAGs). Including IL-22, our screen identifies dozens of genes that limit CNS regeneration. Suppression of these genes in the context of axonal damage could support improved neural repair.

Graphical Abstract

*Correspondence: stephen.strittmatter@yale.edu.

AUTHOR CONTRIBUTIONS

Conceptualization, J.A.L., N.M.T., J.R.S., and S.M.S.; methodology, J.A.L., N.M.T., D.M.C., Y.F., R.K., Y.S., X.W., I.-J.K., and S.M.S.; investigation, J.A.L., N.M.T., D.M.C., K.D., R.K., Y.F., Y.S., X.W., and M.W.; writing – original draft, J.A.L. and S.M.S.; writing – review & editing, all authors; funding acquisition, S.M.S.; resources, S.M.S; supervision, J.A.L., J.R.S., and S.M.S.

DECLARATION OF INTERESTS

The authors declare no competing interests.

SUPPLEMENTAL INFORMATION

Supplemental Information can be found online at https://doi.org/10.1016/j.celrep.2021.108777.

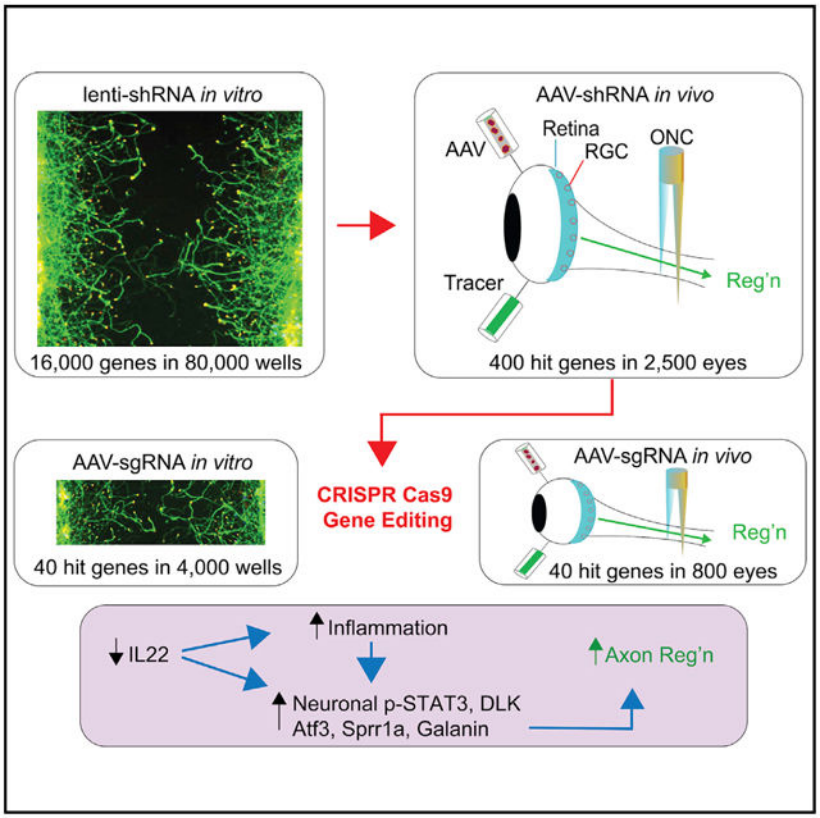

In brief

Lindborg et al. conduct an unbiased, *in vivo*, loss-of-function shRNA-AAV screen of nearly 400 candidate genes for optic nerve regeneration and confirm their role by AAV CRISPR-Cas9 gene editing. Together, their studies uncover 40 axon-regeneration-limiting genes and define a multifactorial role for IL-22 in limiting CNS regeneration.

INTRODUCTION

Neuronal injuries cause debilitation and pain with few palliative options and no curative treatments. Achieving neuroprotection and neuroregeneration after injury remains a challenging and elusive goal. Glaucoma is characterized by retinal ganglion cell (RGC) axon degeneration and cell death, with vision loss (Weinreb et al., 2014), and overlaps with experimental optic nerve crush (ONC) (Templeton and Geisert, 2012). After ONC injury, less than 1% of spared axons regenerate and more than 80% of RGCs die (Nadal-Nicolás et al., 2015; Tran et al., 2019).

Although no intervention achieves full recovery, much has been learned about why axons fail to recover. Glial-based mechanisms extrinsic to neurons, including scar-derived chondroitin sulfate proteoglycans and myelin-associated inhibitors, have a substantial role (GrandPré et al., 2000; McKeon et al., 1991; McKerracher et al., 1994; Wang et al., 2002). Chondroitinase ABC augments axon sprouting and functional recovery after spinal cord injury (Bradbury et al., 2002; Cafferty et al., 2007; Massey et al., 2006). Targeting of

individual myelin proteins or axonal Nogo receptor NgR1 enhances axon growth and functional recovery after CNS injury (Bregman et al., 1995; Fischer et al., 2004; Fournier et al., 2001; GrandPré et al., 2002; Wang et al., 2011, 2020a; Zai et al., 2011). Limited glial production of growth-promoting extracellular molecules also diminishes axon growth. For example, activators of the Jak-Stat pathway significantly enhance cultured RGC neurite outgrowth and neuronal survival (Leibinger et al., 2009).

Separate from the axon's extracellular environment, adult central nervous system (CNS) neurons have limited intrinsic ability to regenerate axons. In contrast, peripheral nervous system (PNS) neurons respond adeptly to axotomy with upregulation of regeneration-associated genes (RAGs) and substantial regeneration. Strong induction of Atf3 (activating transcription factor 3) and Sprr1a (small proline-rich repeat protein 1a) demarcate the enhanced regeneration of axotomized PNS neurons (Bonilla et al., 2002; Hyatt Sachs et al., 2007; Starkey et al., 2009; Tsujino et al., 2000). Enhancing the intrinsic growth potential of RGCs leads to greater axon regeneration. Suppression of neuronal Pten (phosphatase and tensin homolog) or Socs3 (suppressor of cytokine signaling 3) expression disinhibits the Akt/mTOR and Jak-Stat signaling pathways, respectively, to support axon regeneration (Park et al., 2008; Smith et al., 2009). However, incomplete axonal restoration and the challenges of functional recovery compel more complete discovery of axon regenerative mechanisms.

Previously, we surveyed the mouse genome in an unbiased approach for loci that affect axon regeneration (Sekine et al., 2018). Using lentiviral short hairpin RNAs (shRNAs) to survey 17,000 genes after cortical neuron axotomy, we identified more than 400 genes whose suppression supported axon regeneration. Here, we leverage those *in vitro* results to characterize pathways that can be targeted to improve CNS neural repair *in vivo*. Using shRNA-AAV (adeno-associated virus) and CRISPR-AAV-mediated inhibition, we assayed 392 genes and identified 40 targets whose loss-of-function after ONC produced enhanced RGC regeneration. We studied one gene, interleukin-22 (*IL22*), in greater detail because of its bioinformatic linkage to the Jak-Stat signaling pathway and robust effects in multiple tests. We find that IL-22 inhibition leads to increased transcription factors, cytokines, and proteins critical for CNS regeneration. Conversely, exogenous IL-22 application abrogated expression of many pro-inflammatory and pro-regenerative factors. Together, our studies uncover more than three dozen genes limiting axon regeneration *in vivo* and define a multifactorial role for IL-22 in limiting axon regeneration.

RESULTS

In vivo screen of candidate regeneration limiting genes by shRNA-mediated gene silencing

Previously, we screened about 17,000 mouse genes for their functional role in CNS axonal regeneration, identifying more than 400 genes whose suppression via lentiviral shRNA knockdown stimulated regeneration in cortical neuron cultures after injury (Sekine et al., 2018). Here, we tested 392 of those genes individually by *in vivo* loss-of-function in optic nerve regeneration with delivery of recombinant AAVs expressing specific shRNA and GFP (Figure 1A; Table S1). High infection efficiency and minimal provocation of an immune response make AAVs an attractive option for knockdown and editing in animal studies

(Daya and Berns, 2008). The shRNA sequence for a particular gene was selected based on the highest regeneration score from the *in vitro* regeneration screen. ONC surgeries were preceded, 14 d earlier, by intravitreal injections of shRNA-AAV and followed 14 d later by injection of cholera toxin β (CTB) subunit conjugated to a fluorescent dye to anterogradely trace axons (Figure 1B). Efficient transduction of retinal cells, including RGCs, was achieved with recombinant AAV serotype 2/2 (Hellström and Harvey, 2011; Leaver et al., 2006; Petrs-Silva et al., 2009), and AAV infection was confirmed with a GFP reporter in retina whole mounts (Figure S1A). Regeneration of CTB-labeled axons in the optic nerve extending 500 μm distal to the crush site for 392 genes was counted for an average seven nerves per gene, from 2,851 separate eyes (Figure 1C). The scrambled-sequence control background averaged eight axons (5.8–10.6, 95% confidence interval) compared with a positive control from Pten knockdown of 148 axons (111–186, 95% confidence interval) (e.g., Park et al., 2008; Yungher et al., 2015; Zukor et al., 2013).

This screen identified 40 genes with increased regeneration phenotypes relative to the control, as defined either by significant increases of the average number of axons compared with the scrambled sequence ($p < 0.05$) or by an average more than one control standard deviation above the scrambled value (Figures 1C–1E; Table S2). Of interest, Rassf3 and Tbc1d22b are two of several genes whose inhibition had the most significant effect on axon regeneration with counts nearly six times greater than that of the control. Rassf3 is a protein associated with the Ras family of small GTPases having a central role in RAF/MEK/ERK signaling-mediated mechanisms of neuronal survival and repair (Zhong, 2016), whereas Tbc1d22b is part of the Rab-GTPase-activating protein domain with an as-yet-unknown Rab protein association (Ishibashi et al., 2009). Rab proteins have been implicated in axonal growth (Hernández-Deviez et al., 2004), and our unbiased genome-wide cortical neuron regeneration assessment revealed a functional role for 10 different Rab proteins in axon regeneration (Sekine et al., 2018). These findings affirm the translatability of our *in vitro* to *in vivo* regeneration screens and highlight 40 promising regeneration-limiting genes to target for further study.

Axon regeneration after editing of regeneration-limiting genes by CRISPR-Cas9

Having identified multiple *in vivo* axon regeneration phenotypes by shRNA knockdown, we further assessed those genes by CRISPR-Cas9 gene editing as validation of the shRNA knockdown phenotypes. To that end, we employed the dual-vector CRISPR system that packages single-guide RNA (sgRNA) and Cas9 (from *Streptococcus pyogenes*) cassettes in different viral vectors (Figure 2A; Table S3; Swiech et al., 2015). Cas9 expression is driven by the Mecp2 promoter, which isolates gene editing to neuronal populations. An sgRNA species targeting the bacterial enzyme β-galactosidase (LacZ) was used as a non-targeting control. Mouse cortical neuron cultures from P1 pups were used to quantify editing at the DNA, RNA, and protein levels. Neurons were co-transduced with sgRNA-AAV and Cas9-AAV at 3 d *in vitro* (DIV) and harvested for downstream applications at DIV17. The culture composition was 80% $NeuN^+$ neurons, with the remaining cells being 8% $GFAP^+$ (glial fibrillary acidic protein positive) astrocytes and 12% $PDGFRa^+$ or $O4^+$ oligodendrocyte lineage cells (Figure 2C). An 81% cortical neuron transduction efficiency was achieved with AAV serotype 2/1 (Figure 2B, Hammond et al., 2017). Two to five sgRNA species were

generated for each gene because of variability in editing efficiency. For Pten, two sgRNAs, Pten-1 and Pten-3, showed remarkably different editing efficiencies at the DNA (Figure 2D), mRNA (Figure 2E; Table S4), and protein levels (Figure 2F). The reduction of DNA, mRNA, and protein for the Pten-1 versus Pten-3 species was 15% versus 82%, 32% versus 78%, and 80% versus 98%, respectively. Pten-3 (referred to hereafter as “Pten”) produced greater editing overall and was, therefore, selected for use in subsequent assays.

It is worth noting that although DNA editing efficiency was low for the Pten-1 species, its minimal disruption in the Pten locus was sufficient to cause a significant decrease in protein expression. Likewise, for the positive regeneration gene Rassf3, minimal disruption at the sgRNA-targeted DNA locus supported substantial protein reduction (Figure 2G). These findings support the view that downstream changes in protein expression, rather than DNA, may be more of an appropriate readout of editing efficiency, consistent with previous studies (Nelson et al., 2016; Swiech et al., 2015).

Subsequently, all 40 genes were tested in the cortical neuron regeneration assay using the CRISPR system (Figure 2H; Table S2). Axons were injured at DIV17 using a pin tool and analyzed for regeneration using anti-βIII-tubulin staining at DIV25. sgRNA-AAV targeting enhanced regeneration to a statistically significant level for 28 of the 40 genes, compared with the non-targeting LacZ control.

Next, we analyzed *in vivo* regeneration after sgRNA-AAV delivery (Figure 3A) using the viral injection and ONC injury model outlined for shRNA studies in Figure 1B. Because dual AAV injections may reduce infection efficiency *in vivo* (Carvalho et al., 2017), we used Cas9 transgenic mice in conjunction with single AAV delivery of sgRNAs at 10^{12}–10^{13} genome copies/mL. Transgenic mice express Cas9 endonuclease driven by a CAG promoter (Figure 3B), which expands the probability of editing in non-neuronal populations. Intravitreal injection of AAV serotype 2/2 is selective for the retinal ganglion layer (Leibinger et al., 2013a), but it can also infect Müller glia in the inner nuclear layer with a lower efficiency (Liang et al., 2003; Pang et al., 2008). Approximately 50% of RGCs were infected with any given sgRNA-AAV, as judged by GFP overlap with Rbpms antigenicity (Figures S1B and S1D), and, consistent with previous reports (Leibinger et al., 2013a), about 90% of AAV2-infected cells were RGCs (Figures S1C and S1D). Thus, direct effects on RGCs are likely to predominate, but we cannot completely rule out cell non-autonomous effects.

Optic nerve analysis for the 40 genes using CRISPR editing highlighted nine genes with significantly more regeneration phenotypes compared with LacZ (Figures 3A and 3C; Table S2). Only two sgRNA species were generated for most of the 40 genes, and likely, the reduction in the number of positive regeneration hits compared with shRNA can be attributed to the selection of suboptimal targeting sequences. Of the positive regeneration genes using sgRNA, the four most potent were Myl10 (myosin light chain 10), Airn (antisense of insulin growth factor 2 receptor [Igf2R] non-protein coding RNA), Prg2 (proteoglycan 2, proMBP), and IL-22. All showed comparable axon regeneration to Pten, in addition to axon extension well beyond the 500-μm distance of measurement (Figure 2E). IL-22, a cytokine that participates in Jak-Stat signaling, (Leibinger et al., 2013a, 2013b),

consistently showed robust loss-of-function regeneration phenotypes with *in vitro* and *in vivo* models. The activity of Myl10 is consistent with actin-myosin interactions in neuronal growth cones (Jian et al., 1996), Airn with IGF2 signaling (Santoro et al., 2013), and Prg2 with axonal growth and IGF signaling (Glerup et al., 2006; Overgaard et al., 2000; Weyer and Glerup, 2011). The roles of myosin and IGF in PNS and CNS regeneration and repair are well documented (Dupraz et al., 2013; Rabinovsky, 2004; Toy and Namgung, 2013; Wang et al., 2020b). Critically, this *in vivo* screen has identified many genes not previously linked to axon regeneration; all of which were identified by genome-wide shRNA screening *in vitro*, confirmed by *in vivo* knockdown studies in a different CNS population, and validated by gene editing both *in vitro* and *in vivo*.

Effect of axon regeneration gene editing on RGC survival

Some axon regeneration-promoting genes, such as DLK (dual leucine zipper kinase), and regeneration-inhibiting genes, such as Pten, participate in axotomy-induced RGC death (Park et al., 2008; Watkins et al., 2013). Therefore, we considered whether the CRISPR gene editing leading to enhanced regeneration after injury might be linked to changes in RGC survival. We assayed the number of RGCs 14 d after ONC, when approximately 80% of these neurons have undergone apoptosis (Berkelaar et al., 1994; Nadal-Nicolás et al., 2015; Tran et al., 2019). Survival was measured after sgRNA-AAV-targeting of the top six regeneration genes identified in Figure 3A. Retinal whole mounts were stained with Rbpms, a pan-RGC marker (Kwong et al., 2011), and the number of RGC^{+} cells were counted in each of the four retinal quadrants (Figures S2A and S2B) and expressed as a percentage of the total number of RGCs in the uninjured retina (Figure S2C). As expected, only 25% of RGCs survived after injury in sgRNA-LacZ-injected retinas. In line with previous findings (Park et al., 2008), Pten loss-of-function salvaged a significant fraction of the RGC population (34% survival). Although we report smaller increases in RGC survival after Pten inhibition than the described literature using $Pten^{fl/fl}$ mice and AAV-Cre delivery (45% in Park et al., 2008), this gap can be attributed to the different models used and the achieved degree of editing. In addition to Pten, editing of Xylt1 (xylosyltransferase1) rescued a small but significant percentage of RGCs from death. Editing of Myl10 showed a trend toward increased RGC numbers 14 d after injury, whereas IL-22, Prg2, and Airn did not alter survival. Reduction of Rassf3 expression significantly lowered survival, suggesting it has opposing effects on survival and regeneration.

To compare the strength of gene effects on regeneration and survival, the *in vivo* axon regeneration was normalized to RGC survival as a ratio (Figure S2D). Five genes had a regeneration index, per surviving RGC, equal to or greater than Pten, demonstrating improved axon regeneration irrespective of RGC survival, even for the presumptive survival-promoting Myl10 editing. For Xylt1, we observed a survival effect comparable to Pten, but a weaker effect on regeneration. In our recent single-cell RNA sequencing (scRNA-seq) dataset of adult mouse RGCs (Tran et al., 2019), Xylt1 was the mostly highly expressed in intrinsically photosensitive RGCs. However, it is unclear whether the survival and regeneration effects were specific to that population.

Axotomy regulation of regeneration-limiting gene expression

Insight into injury-induced gene expression changes and pathways shared with known axon regeneration genes may inform us about general mechanisms of repair. Our recent RGC scRNA-seq dataset analyzed genome-wide expression patterns across 46 adult mouse RGC types before and after ONC (Tran et al., 2019). We first used this dataset to assess expression in control RGCs. Transcripts for 248 of the 392 (63%) targeted genes assayed in Figure 1C had detectable expression profiles in RGCs (Figure 4A; Table S5). Of the 40 positive regeneration hits in Figure 1D; 24 (60%) are expressed in at least 1% of the RGCs. We next assessed whether any of the 40 genes exhibited altered expression after injury. All genes detected in the control cells were also observed after injury, and none of the 40 positive regeneration hits overlapped with the global differentially expressed genes (771 genes) identified in our scRNA-seq dataset (Tran et al., 2019; Figure 4B; Table S6). Thus, the current screen identified targets whose expression is not globally altered by axonal injury, although some genes (e.g., Xylt1) were upregulated in a small subset of cells (Figure 4C). This finding was, perhaps, not unexpected, as previously described genes with inhibitory roles in RGC axon regeneration (e.g., Pten), also sustain relatively constant baseline expression levels with injury (Tran et al., 2019). In contrast, many RAGs and cell death-associated genes are upregulated after injury. We also observed an overall reduction in target gene expression level and the fraction of RGCs that expressed the target gene after ONC compared with that of the control, which was anticipated because of their degenerative state. The finding that more than 60% of the positive-regeneration gene targets have significant expression profiles in RGCs is consistent with the simplest model for their action, namely, intrinsic modulation of RGC regenerative potential. For genes with minimal (Table S6) or undetected (Table S7) expression in this dataset, two possible explanations are that either they inhibit regeneration non-cell autonomously or simply that their expression in RGCs was below detectable threshold by this method. Further characterization of their expression by more-sensitive methods (i.e., tissue immunostaining, *in situ* hybridization, or different mRNA profiling methods) will be required to distinguish those possibilities.

The 40 genes limiting *in vivo* axonal regeneration were analyzed for enrichment in protein-protein interaction (PPI) networks (Figure 4D). No overall statistically significant enrichment was detected among those genes using STRING database (PPI enrichment p value = 0.709). However, network analysis identified cytokine signaling among four of the genes (IL-22, Socs4, IL-17c, and IL-17Rb), and network expansion highlighted Jak-Stat signaling (Figure 4E). Stat3, a key player in this pathway, is a recognized regulator of regeneration (Qiu et al., 2005). Among the four genes with involvement in Jak-Stat signaling, IL-22 editing showed the most significant regeneration phenotype *in vivo* (Figures 3A and 3C). Therefore, we explored the mechanism by which IL-22 editing supports optic nerve regeneration in more detail.

Expression of IL-22 and related signaling components

To initiate analysis of IL-22, we assessed the RGC expression profile of IL-22 and its co-receptors, IL-10Rb and IL-22Ra1 (Kotenko et al., 2001; Xie et al., 2000). IL-22 and IL-10Rb were expressed at low levels in RGCs but were present across many RGC types (Figure S3A). Uninjured whole-retina RNA-seq analysis of IL-22 levels reports expression

in multiple neuronal populations, including RGCs, amacrine cells, rods, cones, and bipolar cells (Figure S3B; Macosko et al., 2015; Shekhar et al., 2016; Tran et al., 2019; Yan et al., 2020). Low or absent levels of IL-22 are found in non-neuronal cell populations. Because AAV2/2 delivery of sgRNA targets predominantly RGCs (approximately 90%; Figures S1C and S1D), we asked whether the *IL22* gene was edited specifically in RGCs after *in vivo* AAV delivery of IL-22 sgRNA. AAV-infected GFP^+/$Rbpms^+$/$Brn3a^+$ RGCs were collected by fluorescence-activated cell sorting (FACS) 14 d after intravitreal injection. With targeted next-generation sequencing of a 302-bp PCR amplicon, we confirmed indel mutations in the IL-22 locus of RGCs; most of which displayed a single base-pair insertion or deletion (Figures S4A–S4C). Editing of RGCs at the DNA level translated into a significant reduction of IL-22 protein in the total retina using ELISA (Figure S4D) and immunoblotting (Figure S4E), resulting in a large increase in the number of regenerating RGC axons under those conditions (Figure 3A).

In contrast to expression of IL-22 and IL-10Rb, IL-22Ra1 expression was not detected in RGCs (data not shown). Immunostaining with an anti-IL-22Ra1 antibody indicated that IL-22Ra1 expression is chiefly restricted to the ganglion cell layer (GCL) but did not colocalize with $Rbpms^+$ RGC somas or IL-22-sgRNA-infected GFP^+ cells (Figures S3C–S3E). Visualization of the $GFAP^+$ glial population, which does express IL-10Rb (Burmeister and Marriott, 2018; Shekhar et al., 2016), showed some astrocytes with $GFAP^+$ filaments surrounded by IL-22Ra1, although colocalization was not observed (Figure S3E, left inset). Indeed, there were some $IL\text{-}22Ra1^+$ cells spatially distinct from $GFAP^+$ astrocytes (Figure S3E, right inset). These data suggest that IL-22 released from neurons (RGCs or other neuronal cells) may limit axon growth by autocrine signaling via RGC-expressed IL-10Rb, by paracrine signaling via immune or glial-expressed IL-22Ra1, or by a combination of both modalities. Regardless, the apposition and confinement of IL-22, IL-10Rb and IL-22Ra1 expression to the GCL supports the hypothesis that axon regeneration triggered by IL-22 inhibition is initiated from RGC-intrinsic changes of the secreted cytokine and local action within the GCL.

IL-22 editing initiates a pro-regenerative transcriptional program including Stat3, DLK, and RAGs

A hallmark of successful nerve regeneration after injury is the stimulation of a neuron's intrinsic growth capacity (Ma and Willis, 2015). Because RAG upregulation is often a clear indication of the regenerative state of neurons, we evaluated how effectively IL-22 inhibition primed RGC neurons to regenerate. Transcriptional activation of RAGs was measured 3 d after injury. We observed a 2-fold increase in *Atf3* mRNA in edited retina compared with unedited retina, in addition to marked 4-fold and 3-fold increases in *Sprr1a* and *Galanin* transcripts, respectively (Figure 5A). Furthermore, a substantial increase in Atf3 immunoreactivity was observed in the GCL of IL-22-edited retinas 3 d after injury compared with non-targeting LacZ (Figure 5B).

We next sought to identify signaling changes that link IL-22 suppression to RAG activation. Stat3 is a key factor in promoting axon regeneration, in large part via its upregulation of RAG expression (Mehta et al., 2016; Smith et al., 2011). *Stat3* transcript levels were

quantified 3 d after ONC (Figure 5C). Both LacZ- and IL-22-edited retinas displayed a marked increase over their respective uninjured controls, but a significantly larger increase in *Stat3* was detected in injured and IL-22-edited retina compared with the non-targeting injured control. The retinal distribution of phosphorylated Stat3 (p-STAT3) 14 d after injury was localized predominantly in RGCs in the GCL of IL-22-edited retinas (Figure S5A). Astrocytes also expressed p-STAT3 after injury (Figure S5B). Similar to RGC-specific p-STAT3 expression, induction of p-STAT3 in astrocytes has historically been shown to support neuronal regeneration in acute models of injury (Anderson et al., 2016). Assessment of the total protein levels in the retina confirmed that IL-22 inhibition significantly enhanced p-STAT3 expression 14 d after ONC compared with injured control retina (Figure 5D). Remarkably, injection of sgRNA-AAV targeting IL-22 was sufficient to cause significant enrichment of activated p-STAT3 protein, with levels exceeding that observed in injured and unedited retina. Thus, IL-22 editing partially bypasses the requirement for injury to drive Stat3 activation.

We considered whether endogenous IL-22 levels were at saturating concentrations with respect to that of post-axotomy RAG expression by injecting excess recombinant IL-22 (r-IL-22) into the vitreous. r-IL-22 was injected 1 d before injury because marked increases in IL-22 protein were detected in the retina at that post-injection time point compared with the PBS-injected control retina (Figure 5E), which made it suitable for assessing the effects of increased IL-22 on RAG expression. Four days after r-IL-22 injection and 3 d after injury, we measured retinal *Stat3* and RAG transcript expression in comparison to that of control and IL-22 loss-of-function gene-edited retina (Figure 5F). Increased levels of retinal IL-22 significantly diminished *Atf3* expression relative to both the control and the IL-22-edited eyes. For other RAGs and *Stat3*, excess IL-22 retina yielded expression levels significantly less than it did for sgRNA-IL-22 retina, and non-significantly less than it did for control eyes. These data define a monophonic function for suppression of Stat3 and RAG expression by IL-22 after axotomy, which nears saturation at physiological levels of IL-22.

In addition to Stat3, induction of RAG expression is aided by the retrograde transport of injury-induced axonal signals (Ben-Yaakov et al., 2012; Cox et al., 2008). DLK is one such critical signal that not only engages RAG cascade activation but also ferries axonal p-STAT3 to the cell body to augment a neuron's pro-regenerative program (Shin et al., 2012). Because DLK has also been shown to initiate regenerative responses in RGCs (Watkins et al., 2013), we evaluated its expression in the retina 3 d after injury. scRNA-seq analysis of *Dlk* expression in RGCs revealed a non-significant trend to increase early after injury with a decrease by 4 days after ONC (Figure 6A; Tran et al., 2019), most likely because of the initiation of RGC death. In line with our scRNA-seq dataset, unchanged levels of *Dlk* transcripts were measured between uninjured and injured control retinas 3 d after injury, and a slight yet significant increase in transcript levels between uninjured and injured IL-22-edited samples (Figure 6B). Injection of r-IL-22 did not significantly alter expression compared with control baseline (Figure 6C). Notably, significant increases in DLK protein were observed with IL-22 editing 14 d after injury by immunoblotting (Figure 6D). Few DLK^+ cells were observed in the GCL of control retinas compared with that of IL-22-edited retinas 14 d after injury (Figure 6E). After injury and IL-22 inhibition, DLK expression increases in both βIII-tubulin$^+$ neuronal and $GFAP^+$ non-neuronal populations in the GCL.

Those cellular expression patterns of DLK are similar to the findings in the uninjured whole-retina RNA-seq datasets, in which DLK is expressed in all retinal cell types (Figure S5C; Macosko et al., 2015; Shekhar et al., 2016; Tran et al., 2019; Yan et al., 2020). Here, we find that a population of neurons in the GCL upregulate DLK after IL-22 editing, and these molecular changes are concurrent with enhanced regeneration of RGC axons. Taken together, these results suggest that amplified expression of RAGs after IL-22 inhibition is driven by both increased DLK and activated Stat3. This triad of neuronal changes that occur because of IL-22 editing demonstrate a shift of RGCs to a primed regenerative state.

Potential mediators of Stat3 activation after IL-22 inhibition

To establish a connection between IL-22 suppression and Stat3 activation, we surveyed retinal expression of multiple Stat3-activating cytokines in response to IL-22 loss. Early transcript changes were analyzed 3 d after ONC in IL-22-edited and unedited retinas (Figure 7A). *Lif* mRNA was significantly increased by 3-fold in injured IL-22-edited retinas compared with the control. Importantly, Lif is a member of the glycoprotein-130 (gp130)-activating cytokine family, which is neuroprotective and activates Stat3 (Leibinger et al., 2009, 2013a). IL-22 silencing also stimulated a 6-fold and a significant 13-fold increase in *Il1β* and *Il6* mRNA transcripts, respectively, over injured LacZ control. IL-6, similar to Lif, is a member of the gp130 cytokine family that activates Stat3 and promotes axon regeneration in both CNS and PNS neurons (Cao et al., 2006; Leibinger et al., 2013b; Yang et al., 2012). IL-22 belongs to a family of cytokines that includes IL-10, IL-19, IL-20, and IL-24 (Sabat, 2010), all of which signal via the Jak-Stat3 pathway (Kiu and Nicholson, 2012; Kragstrup et al., 2018). Of those, we observed large transcript increases across all species after IL-22 editing and injury compared with the injured control. Most notably, *Il10* and *Il24* boasted transcript increases six times and 28 times, respectively, higher than that of LacZ. Clearly, loss of IL-22 stimulates a shift in the expression of cytokines that are well known in their role of potentiating Stat3 activation leading to axon regeneration.

The increased expression of pro-inflammatory cytokines suggests an enhanced immune reaction in response to the loss of IL-22. Therefore, we evaluated markers of immune and glial cell activation after IL-22 editing in the injured retina. Substantial increases in transcript expression of the microglia/macrophage chemokine *Ccl2* was observed 3 d after ONC in IL-22-edited retinas compared with that of the control (Figure 7B). These microglia/macrophage injury-induced changes were concurrent with significant increases in *Cd68* transcript levels in both edited and unedited retinas, but a larger increase was observed after IL-22 inhibition. Notably, IL-22 editing was sufficient to cause a significant increase in *Ccl2* transcript over that of LacZ in uninjured tissue, suggesting possible changes in cell chemotaxis or activity before injury. The observed increases in *Ccl2* mRNA with IL-22 loss are supported by a prior study that reported reduced *Ccl2* transcript in the retina after intravitreal injection of recombinant IL-22 (Mattapallil et al., 2019). Significant increases in mRNA for injured, unedited and IL-22-edited retinas, compared with their respective uninjured controls, were also observed for the reactive astrocytic indicator *Gfap*, although no differences between injection groups were noted. Evaluation of GFAP in the retina 3 and 14 d after ONC did not reveal any differences in astrocyte reactivity between IL-22-edited and unedited retinas (Figures S6A and S6B).

Greater immune cell activity after IL-22 inhibition

To characterize the immune cell response to IL-22 suppression, we analyzed the localization of microglia/macrophages among retinal layers after injury. Their distribution showed a specific cellular migration pattern for both LacZ and IL-22 groups, with accumulation in the outer plexiform layer at 3 d, extending ventrally to the GCL at 14 d after injury (Figures 7E, 7F, S6C, and S6D). This effect, however, was more pronounced after IL-22 editing in which almost all microglia/macrophages were confined to the GCL. The localization of microglia/macrophages to the inner and outer plexiform layers early after injury has been described as a process that is related to microglial function in regulating retina synapse formation and refinement during development (Li et al., 2019; Santos et al., 2008). Retinal injury and degeneration similarly result in reorganization of synapses requiring regulation by microglia (Silverman and Wong, 2018). In addition to the divergent patterns of microglia/macrophage localization among injection groups, clear distinctions in their accumulation and activation were apparent among injured groups. Iba1$^+$ (Figures 7C and 7E) and CD68$^+$ (Figures 7D and 7F) populations were evaluated at both 3 and 14 d after crush injury. Significantly more of both Iba$^+$ and CD68$^+$ cells were identified after IL-22 editing at 3 d after ONC compared with LacZ, although numbers were comparable between groups at the later time point. These data suggest that, compared with the control, IL-22 inhibition drives earlier microglia/macrophage accumulation and activation. The normalization of the cellular inflammatory response to control levels mirrors the reduction 14 d after ONC in transcript levels of the proinflammatory factors evaluated in Figure 7 (data not shown).

We also examined the effect of excess IL-22 on inflammation in the retina. r-IL-22 was injected intravitreally into wild-type (WT) mice 1 d before ONC. Supplementation with r-IL-22 reversed the inflammatory transcriptomic profiles observed in the retina with both control injections and with IL-22 inhibition (Figure 7G). Specifically, significant reductions in *Cd68*, *Tnfα*, and *Il1β* transcripts compared with the control underscored an overall trend in the expression of pro-inflammatory factors because of IL-22 expression. Moreover, neither microglia/macrophage nor astrocyte accumulation or activation were significantly altered 3 d after ONC with enhanced IL-22 levels compared with that of the PBS control (Figures S7A–S7E). Although glial composition was unaffected by injection of r-IL-22 early after injury, changes in the production of pro-inflammatory and pro-regenerative indicators define the contribution of IL-22 to the injury response. Overall, these studies indicate that titration of IL-22 levels dampens the inflammatory response after injury and suppresses the transcriptional expression of important Stat3 activators contributing to enhanced RAG expression and ultimately, axon regeneration.

DISCUSSION

We applied genome-wide *in vitro* and *in vivo* loss-of-function screening methods to define mechanisms of adult mammalian CNS axonal regeneration. We began with a set of about 400 genes identified previously by our unbiased and comprehensive loss-of-function screening of the mouse genome (Sekine et al., 2018). Using both shRNA and CRISPR viral-mediated gene targeting, we distilled that list to 40 genes whose loss of function enhanced regeneration *in vivo*. Although the *in vivo* shRNA screen provided 40 axon regeneration-

limiting genes, the results of the sgRNA screen of those 40 genes yielded 28 *in vitro* confirmations and 9 *in vivo* confirmations. The lack of exact matching between the two methods is likely attributable primarily to the selection of shRNA or sgRNA sequences. Notably, five or more shRNAs were evaluated for each gene for the *in vitro* screen of Sekine et al. (2018). The most effective shRNA sequence was used here for optic nerve regeneration. Conversely, an average of only two sgRNAs were generated for most of the 40 genes, and likely, the reduction in the number of positive regeneration hits compared with that of shRNA can be attributed to suboptimal targeting sequences. As an example, efficiency for PTEN suppression varied widely with different sequences.

Here, single regeneration targets that emerged from the 40-gene list included Myl10, Airn, Prg2, Rassf3, Tbc1d22b, and Xylt1. Literature regarding the function of Myl10 is scarce, but myosin light chain kinase has been shown to regulate actin-myosin interactions in neuronal growth cones (Jian et al., 1996). Given that myosin light chains are substrates for myosin light chain kinase (Tan and Leung, 2009), we hypothesize that Myl10 controls extension and retraction of regenerating axons. Airn is an RNA that paternally silences the Igf2R gene (Santoro et al., 2013), whose unimpeded function is to bind and traffic Igf2 for lysosomal degradation (Oka et al., 1985; Wang et al., 1994). Although Igf1 enhances RGC survival after ONC (Bray et al., 2019), the mechanism of IgfR2/Igf2-regulated axon regeneration requires further study. Prg2 is a secreted glycoprotein known to bind heparan sulfate proteoglycans (Glerup et al., 2006), which regulate axonal growth. Prg2 also forms a complex with the protease PAPP-A (Overgaard et al., 2000), which releases active IGF-I from its antagonistic binding protein IGFBP-4,5 (Weyer and Glerup, 2011). Thus, the role or Prg2 in axon-limiting axonal regeneration may relate to IGF. Rassf3 is consistent with Ras/RAF function in neuronal survival and repair (Zhong, 2016) and with Tbc1d22b in Rab-GTPase regulation of axonal regeneration (Hernández-Deviez et al., 2004). Xylt1 encodes a key enzyme in the synthesis of chondroitin sulfate proteoglycans (Esko et al., 1985; Müller et al., 2006; Prante et al., 2006), so its suppression should reduce those extracellular inhibitors.

Here, we focused on IL-22 for two reasons. First, it was one of the strongest hits and was consistent across knockdown methods. Second, IL-22 is a cytokine regulating Jak-Stat signaling, which is implicated in nerve regeneration. Although the role of IL-22 had not been explored until now, we explored the Jak-Stat pathway to delineate that cytokine's mechanism of action. Our results place IL-22—alongside Stat3, DLK, and RAG expression (Bollaerts et al., 2017)—as a critical node in the inflammatory response to nerve injury. Analysis of IL-22 inhibition revealed that endogenous IL-22 suppresses the inflammation after ONC and prevents upregulation of Stat3 activators DLK and RAGs. In the retina, enhanced inflammation induced by ONC and lens injury or injection of the Toll-like receptor 2 (TLR2) agonist zymosan elicits a regenerative RGC response (Leon et al., 2000; Yin et al., 2003), which is due, in large part, to glial activation and release of growth-promoting factors, such as Lif and IL-6, which stimulate Stat3 and RAG expression in RGCs (Leibinger et al., 2009, 2013a, 2013b). Mechanistically, we propose that IL-22 limits cytokine signaling and inflammation at the baseline and after axotomy. Before injury, IL-22 has little effect on glial or neuronal cells in the retina, but it primes an injury response, including Stat3. In mice with endogenous IL-22, ONC induces limited RAG expression for

Atf3, Sprr1a, and Galanin, with a limited inflammatory glial reaction in the retina and minimal regeneration of axons in the optic nerve. After suppression of IL-22, the axotomy signal mediated by DLK and p-STAT3 initiates greater and more-rapid cytokine and growth factor induction as well as glial migration and activation. In that setting, cell-autonomous and/or cell-non-autonomous upregulation of RAGs in RGCs are markedly enhanced and axon regeneration is increased. Further, injection of recombinant IL-22 suppresses cytokine and RAG expression, placing IL-22 as a key regulator of regeneration.

Stat3 activation is essential to bridge inflammation with RAG induction and axon regeneration in both PNS and CNS (Bareyre et al., 2011; Leibinger et al., 2013a; O'Brien and Nathanson, 2007; Pellegrino and Habecker, 2013; Qiu et al., 2005). Although IL-22 can activate Stat3, it has complicated signaling functions (Dudakov et al., 2015). The injury-induced increases in retinal Stat3 transcript and protein after ONC are significantly larger when IL-22 has been silenced. Moreover, IL-22 editing without injury is sufficient to increase expression of *Ccl2*, *Il1β*, *Il6*, and *Il10* transcripts and expression of p-STAT3 protein. Although IL-22 may promote Stat3 activation in other contexts, its loss in RGCs allows compensatory increases of alternate potent Stat3 activators, such as Lif, IL-6, IL-10, IL-19, IL-20, and IL-24 (Leibinger et al., 2009; Martin et al., 2003). Our results indicate that IL-22 actively quells an immune response, consistent with studies of experimental autoimmune encephalomyelitis (Laaksonen et al., 2014) and of experimental autoimmune uveitis (Mattapallil et al., 2019). After ONC, the enhanced cytokine-driven immune response is pro-regenerative. In addition to Stat3, IL-22 inhibition produced marked increases in retinal expression of the injury-induced signal DLK (Watkins et al., 2013).

Recognition of the role of IL-22 in CNS regeneration highlights the cooperation between neuronal intrinsic mechanisms and non-neuronal cells. IL-22 expression is induced by IL-6 and IL-23 (Liang et al., 2006; Zheng et al., 2007) and is found in RGCs and bipolar cells (Figure S3A; Shekhar et al., 2016; Tran et al., 2019). IL-22 signals via the heterodimer IL-22Ra1 and IL-10Rb (Zenewicz and Flavell, 2008). Although expression of IL-10Rb is pervasive in the retina (Boyd et al., 2003), RGC-specific expression of IL-22Ra1 mRNA was below the detection limit here. IL-22Ra1 was more abundant on glial cells, as previously described (Perriard et al., 2015). Thus, RGC release of IL-22 after ONC may act on glia to initiate inflammation and cytokine expression. Paracrine factors may then stifle neuronal-specific increases in activated Stat3, DLK, and RAG expression to attenuate axon regeneration with endogenous IL-22.

In conclusion, IL-22 editing permits disinhibition of inflammation after ONC, leading to the upregulation of growth-promoting transcription factors that stimulate Stat3, DLK, and finally, downstream RAGs, culminating in augmented axonal regeneration. Here, we focused on IL-22, but our *in vivo* screen identified more than three dozen additional genes whose endogenous expression limits axon regeneration. Strikingly, none of those genes were strongly upregulated after axotomy. Therefore, expression surveys may fail to identify many negative regulators of axon regeneration. Future studies of the multiple pathways demonstrated here are expected to provide new molecular avenues to promote neural repair. Importantly, the identification of multiple pathways provides the opportunity for multiplexed gene editing or combined pharmacological interventions.

STAR★METHODS

RESOURCE AVAILABILITY

Lead contact—Further information and requests for resources and reagents should be directed to and will be fulfilled by the Lead Contact, Stephen M. Strittmatter (stephen.strittmatter@yale.edu).

Materials availability—This study did not generate new unique reagents.

Data and code availability—The RGC scRNA-seq adult atlas and ONC datasets analyzed in this study were previously published in Tran et al. (2019). The accession number for these datasets is GEO: GSE137400.

EXPERIMENTAL MODEL AND SUBJECT DETAILS

Mice and surgery—All experiments were performed on healthy mice under protocols approved by the Yale Institutional Animal Care and Use Committee. Male and female (8–12 weeks old) wild-type (C57BL/6J, The Jackson Laboratory) and Cas9 ($H11^{Cas9}$; Chiou et al., 2015; The Jackson Laboratory) mice were used for this study. No notable sex-dependent differences were observed during analysis. Mice had *ad libitum* access to food and water and were housed under a 12 h light/dark cycle. Mice were anesthetized under isoflurane and received bilateral intravitreal AAV injections of 1.5 μL of control or targeted virus. For Il22 gain-of-function experiments, PBS or recombinant Il22 (Peprotech) at a concentration of 200 ng/μl was injected bilaterally into the vitreous cavity (Mattapallil et al., 2019). Fourteen days following AAV injection, mice were anesthetized by intraperitoneal injection of a cocktail of ketamine (100 mg/kg) and xylazine (10 mg/kg). The optic nerves were exposed intraorbitally and crushed for 5 s using jeweler's forceps (Dumont 5, Fine Science Tools) at a location 1 mm posterior to the eyeball (Wang et al., 2015). Alexa 555-CTB (cholera toxin subunit B, Thermo Fisher) was injected intravitreally 14 d post-ONC injury to anterogradely label axons. Mice were killed 3 d later by CO_2 inhalation, and optic nerves and retinas were harvested. The few mice (< 3%) with macroscopic evidence for orbital infection were excluded from analysis.

Cell lines and cell culture—The HEK293T cell line was purchased from ATCC (Manassass, VA). Cells were maintained in DMEM (GIBCO) supplemented with 10% fetal bovine serum (GIBCO) and 1% penicillin/streptomycin (GIBCO). Primary cortical cultures were established from P1 wild-type mice and were prepared as described previously (Sekine et al., 2018). Briefly, meninges were removed from dissected cortices in ice-cold Hibernate E medium (BrainBits) and incubated in HBSS containing 30 U/ml Papain (Worthington Biochemical),1.5 mM $CaCl_2$, 2.5 mM EDTA, and 2 mg/ml DNaseI (Sigma) at 37°C for 20 min. Digested tissues were triturated and suspended in Neurobasal-A (GIBCO). Cells were plated on 96 well tissue culture plates coated with poly-D-lysine at a density of 4.0×10^4 cells per well in 200 μL of Neurobasal-A supplemented with B-27 (GIBCO), GlutaMAX (GIBCO), and penicillin-streptomycin.

METHOD DETAILS

DNA constructs—*shRNA*. The helper-free shRNA expression system (Cell Biolabs) comprised of pHelper DF6, pAAV-RC6, and pAAV-U6-GFP vectors were used. shRNA sequences (Table S1) were cloned at the BamH I and EcoR I (NEB) restriction enzyme sites of the pAAV-U6-GFP expression vector. Non-targeting shRNA was generated as a control (target sequence: CAACAAGATGAAGAGCACCAA). *sgRNA*. The SpCas9 (pX551) and single guide RNA (sgRNA, pX552) expression plasmids developed by the Zhang lab (Swiech et al., 2015) were obtained from Addgene. sgRNA target sequences (Table S3) of 20-nt length were chosen using the CRISPR design tool (https://portals.broadinstitute.org/gpp/public/analysis-tools/sgrna-design), selected to precede a 5′-NGG protospacer-adjacent motif sequence, and prioritized based on minimal off-target effects. A negative control sgRNA sequence targeting the LacZ gene from *E. coli* was generated using the sequence TGCGAATACGCCCACGCGAT. To generate sgRNA-expressing constructs, pX552 was digested using SapI Fast Digest (Thermo Fisher). Annealed shRNA and sgRNA oligos were ligated using T4 and T7 DNA Ligase, respectively (NEB). Transformation was performed using One Shot Stbl3 Chemically Competent *E. coli* (Thermo Fisher). Following maxi prep (QIAGEN), Sanger sequencing confirmed correct shRNA and sgRNA insertion using the U6 promoter sequencing primers (5′ to 3′) TGGACCATCCTCTAGACT and (5′ to 3′) GAGGGCCTATTTCCCATGATTC, respectively.

Transfection of HEK293T cells and AAV vector production—Cells were passaged the day before transfection at a density of 10^7 cells per 15-cm plate and were transfected at approximately 80% confluency. For AAV production, 18 μg of DF6 helper plasmid, 6 μg of sgRNA expression plasmid, and 6 μg of 2/2 or 2/1 serotype packaging plasmid were combined in 3 mL of serum-free DMEM. After addition of 150 μL of the transfection reagent polyethylenimine (PEI, Polysciences Inc.), the DNA:PEI transfection mixture was incubated at room temperature for 15 minutes before adding it to HEK293T cells contained in supplemented DMEM. Lower titer AAV particles using 2/1 serotype plasmid were produced for cortical neuron transduction as described in Konermann et al. (2013). Briefly, 72 h following transfection, the supernatant was collected, filtered using a 0.22 μm cellulose acetate filter (Corning), and stored at −80°C. Concentrated AAV particles for *in vivo* retinal cell infection were obtained using 2/2 serotype plasmid (Pang et al., 2008). Seventy-two hours after HEK293T cell transfection, cells were collected, subjected to repeated freeze-thaw cycles to release viral particles into the supernatant, treated with DNaseI (10 U/ml, Sigma-Aldrich) and benzonase (50 U/ml, Millipore) for 30 min at 37°C, and centrifuged at 3,000 × g for 20 min at 4°C to remove cell debris. AAVs were then purified using iodixanol density gradient ultracentrifugation (Hermens et al., 1999). Viral titers were determined using iQ SYBR Green Supermix (Bio-Rad) and quantitative PCR (Bio-Rad CFX96). Samples were compared against a standard curve derived from a virus of known titer diluted from 10^{13} to 10^8 copies per ml. Average viral titers for cortical neuron transduction experiments were 10^9–10^{10} copies per ml, and 10^{10}–10^{13} copies per ml for *in vivo* infection.

Optic nerve tissue processing and regeneration analysis—Crushed optic nerves were fixed in 4% PFA for 1 h and chemically cleared with BABB (1 part benzyl alcohol, 2

parts benzyl benzoate) using an adapted protocol from Ertürk et al. (2011). Briefly, nerves were rinsed in ddH_2O and then incubated in 50%, 80%, and 100% tetrahydrofuran for 20 min, 20 min and 1 h, respectively, followed by 20 min in 100% dichloromethane. Nerves were then submerged in BABB at 4°C for 1 h until mounted and coverslipped. The number of regenerating axons were counted from each image of approximately 30–40 z stacks using an epifluorescence microscope (Zeiss Axio Imager M2) with a 10x lens. Positive axon counts extended 500 μm distal to the crush site. Representative z stack images were taken at 20x using a confocal microscope (Zeiss LSM 710).

RGC survival—Eyes were removed and fixed in 4% PFA for 1 h at room temperature. Intact retinas were isolated and post-fixed in 4% PFA for 15 min and washed in PBS. Following a 1 h incubation in PBS containing 5% NDS, retinas were incubated with a Rbpms primary antibody (1:1000; PhosphoSolutions, #1830-Rbpms) for 3 d at 4°C. Retinas were subsequently washed in PBS, incubated with an AF555 secondary antibody (1:400; Thermo Fisher) for 1 h at room temperature, and washed in PBS. Four incisions were made from the retinal periphery halfway to the optic nerve to produce a flat preparation, and the whole retinas were mounted on microscopy slides with antifade mounting medium (Vectashield). Cell counts were performed on an Axio Imager M2 (Zeiss) with a 10x objective, and representative images were taken at 40x on a confocal microscope (Zeiss LSM 710). For each retina, 3 fields of equal dimensions were sampled from each of the 4 retinal quadrants (12 fields total). Each field was run though ImageJ's FFT bandpass filter, auto-thresholded, and converted to a binary image. After removing outliers, RGCs were counted using the cell counter. The total number of Rbpms+ RGCs were summed from each field, averaged across 4–5 retinas, and presented as a percentage of Rbpms+ RGCs from uninjured retina.

Primary cortical neuron culture—On DIV17, uninjured cortical neuron cultures were fixed in 4% PFA, and incubated overnight at 4°C with the following antibodies: anti-NeuN (1:500, Millipore), anti-GFAP (1:500, Dako), anti-Iba1 (1:1000, Wako), anti-PDGF Receptor a (1:500, CST), anti-O4 (1:500, R&D Systems). Secondary antibody incubation was performed for 1 h at room temperature using AF488 or AF555 IgG (1:1000, Invitrogen), or AF488 IgM (1:1000, Thermo Fisher). For editing and regeneration studies, cortical neurons were co-transduced with sgRNA-AAV and Cas9-AAV on DIV3. AAV serotype 2/1 was used for efficient transduction of cortical neurons (Hammond et al., 2017). Neurons were collected on DIV17 for DNA, RNA, and protein assays. The axon regeneration assay was performed as described previously with modifications (Huebner et al., 2011). On DIV17, 96-well cultures were scraped using a floating pin tool with FP1-WP pins (V&P Scientific) and allowed to regenerate for another 8 d before fixation with 4% PFA. Regenerating axons in the scrape zone were visualized using an anti-βIII-tubulin antibody (1:2000, Promega) and AF647 secondary antibody (1:1000, Invitrogen). DAPI (Bio-Rad) was used to label nuclei in all experiments. Images were taken on a 10x objective in an automated high-throughput imager (ImageXpress Micro XLS, Molecular Devices) under identical conditions. Image thresholding and quantitation were automated using an ImageJ script.

DNA isolation, T7 endonuclease I (T7EI) assay and indel detection—Cortical neuron DNA was isolated using QuickExtract DNA Extraction Solution (Lucigen) 14 d following transduction with Cas9-AAV and sgRNA-AAV targeting LacZ, Pten-1 or Pten-3. The following primers were used to amplify the Pten locus containing the sgRNA sequences (5′−3′): Pten-1F AGTCCTTACATGGGTTGGTTATG; Pten-1R CTCCTCCTCCCAAGTGTATCT; Pten-3F GCCTTTGCTTATTGGGTTCATAG; Pten-3R TTTGAAGGGCTCCTCTCTTTC. Indel detection was performed with Alt-R Genome Editing Detection Kit (IDT) according to the manufacturer's instructions. Editing efficiency was calculated by measuring the percent reduction of the band intensity of the full-length treated (+T7EI) amplicon relative to the full-length untreated (−T7EI) amplicon.

qPCR—Retinas were harvested and frozen 3 d post-ONC. Total RNA was prepared using RNeasy Plus Mini Kit (QIAGEN) and subjected to RT-PCR using iScript cDNA Synthesis Kit (Bio-Rad). cDNA was used for real-time quantitative PCR with TaqMan gene expression master mix (Applied Biosystems) and prevalidated TaqMan gene expression assays (Applied Biosystems; Table S4) on a Bio-Rad CFX Connect real-time PCR detection system using standard cycles. Each sample was analyzed in duplicate. Relative expression was determined using the Comparative Ct Model (ΔΔCt) with Gapdh as the internal control.

Immunoblotting—Tissue or primary cortical neurons were homogenized using a RIPA Lysis Buffer System (SCBT), and protein concentrations were determined using a Pierce BCA Protein Assay kit (Thermo Fisher Scientific). Protein homogenates were analyzed by SDS-PAGE in 4%–20% Tris-Glycine gels (Bio-Rad). Membranes were blocked in TBST containing 5% BSA for 1 h at room temperature, and subsequently incubated overnight at 4°C with the following antibodies: anti-Pten (1:1000, CST), anti-Il22 (1:1000, Millipore), anti-p-STAT3 (1:2000, CST), anti-DLK (1:1000, Genetex), anti-β-actin (1:2000, CST). Following primary antibody incubation and washing, secondary antibodies (Odyssey IRDye 680 or 800) were applied for 1 h at room temperature. Membranes were then washed and visualized using the LI-COR Odyssey IR imaging system.

ELISA

Retinal concentrations of Il22 were measured using a commercially available kit (R&D Systems). Total protein was isolated from retinas 14 d after ONC, and samples were prepared according to the manufacturer's instructions. Standards, controls, and experimental samples were assayed in duplicate.

Histology and immunostaining—Eyes were harvested and fixed for 1 h in 4% PFA. Following cryopreservation in 10%, 20%, and 30% sucrose at 4°C for 30 min, 2 h and overnight, respectively, eyes were embedded in Tissue-Tek OCT compound (Electron Microscopy Sciences) and sectioned at 10 μm using a cryostat. The following primary antibodies were incubated with tissue sections overnight at 4°C: anti-Iba1 (1:200, Abcam), anti-CD68 (1:250, Bio-Rad), anti-GFAP (1:500, Abcam), anti-DLK (1:100, Genetex), anti-Atf3 (1:200, Novus Biologicals), anti-GFP (1:500, Abcam), anti-Il22Ra1 (1:200, Bioss), anti-Rbpms (1:100; PhosphoSolutions), anti-βIII-tubulin antibody (1:500, Promega). Following primary antibody application and washing, tissue was subsequently incubated in

AF594, AF546, AF647, or AF488 secondary antibodies (1:400; Invitrogen, Thermo Fisher) for 1 h. DAPI (1:1000; Invitrogen) was used to label nuclei. Images were captured using an Axio Imager M2 (Zeiss), a LSM 880 confocal (Zeiss), or a TCS SP8 confocal (Leica). To visualize AAV infection in wholemount retinas, tissue was stained with an anti-GFP (1:500, Abcam) antibody for 3 d at 4°C. Retinas were subsequently washed in PBS, incubated with an AF488 secondary antibody (1:400; Invitrogen) for 2 h at room temperature, and washed in PBS.

FACS sorting, next-generation sequencing and indel detection—Fourteen days after AAV injection with either LacZ or Il22 sgRNA-AAV, single retinas were enzymatically digested in 0.125% collagenase for 1 h at 37°C. Following mechanical digestion and single-cell suspension, cells were washed in FACS buffer (PBS, 1% BSA) and blocked with a monoclonal antibody to CD16/CD32 (1:500, Biolegend) for 10 min at 4°C. Cells were incubated with primary antibodies against Rbpms (1:100, Proteintech) and Brn3a (1:100, Abcam) for 2 h at 4°C, washed, incubated with APC-conjugated secondary antibody (10 μl/10^6 cells, R&D Systems) for 1 h at 4°C, washed, resuspended in FACS buffer, and then sorted and collected using a BD FACSAria II (BD Biosciences) based on expression of GFP, Rbpms, and Brn3a. All events were gated based on viable single cells. DNA was extracted from collected cells using DNeasy Blood and Tissue Kit (QIAGEN), and a 302 bp amplicon that spanned the sgRNA-targeted region in the Il22 locus was generated (5′−3′ F: GAACTCATACTCTCTTGGCTACTC, 5′−3′ R: CATCAGGTAGCACTGATCCTTAG) for each sample. PCR products were submitted to Genewiz for their Amplicon-EZ service (Illumina 2×250 bp platform) to examine the incidence of indels at approximately 50,000 reads per sample.

QUANTIFICATION AND STATISTICAL ANALYSIS

Statistical details of each experiment can be found in the figure legends. The number of experimental replicates (n), and the designation of n belonging to the number of tissues or cells are indicated in the figure legends or outlined in the Method details. Statistical comparisons included one- and two-way ANOVA and Student's t test as specified in the figure legends using Prism software (Graph-Pad version 7.04) or Excel. Statistical significance was set at $p < 0.05$. Data presented in graphs are mean ± SEM unless stated otherwise. All imaging quantifications were conducted by experimenters unaware of experimental group.

scRNA-seq analysis—The RGC scRNA-seq adult atlas and ONC datasets analyzed in this study were previously published in Tran et al. (2019) and the P14 whole mouse retina scRNA-seq dataset in Macosko et al. (2015). Previous tSNE, RGC cell type designations, and processed expression matrixes of atlas and post-ONC RGCs were used. Feature, violin, and dot plots were generated using custom RStudio scripts as previously described (Macosko et al., 2015; Shekhar et al., 2016; Tran et al., 2019). For the scatterplots showing the expression of gene targets (392 queried, 248 plotted), the average number of transcripts in expressing cells was plotted against the fraction of RGCs expressing each gene in RGCs from the atlas dataset and the ONC dataset merged and averaged across all time points (0.5, 1, 2, 4, 7, 14 d post-ONC) using ggplot2. Expression level was defined as (average number

of transcripts in expressing cells) * (fraction of expressing RGCs). For violin plots of the whole retina scRNA-seq dataset, data from clusters corresponding to the six major retinal neuron classes (horizontal cells (HC), bipolar cells (BP), amacrine cells (AC), retinal ganglion cells (RGC), rods and cones, and non-neuronal populations (including Muller glia, astrocytes, fibroblasts, vascular endothelium, pericytes and microglia) were merged and plotted. For these plots, expression level was defined as (average number of transcripts in expressing cells) * (fraction of expressing cell-specific type).

Supplementary Material

Refer to Web version on PubMed Central for supplementary material.

ACKNOWLEDGMENTS

This work was supported by grants from the Falk Medical Research Trust and from the NIH to S.M.S. (U01EY027256, R35NS097283); the NIH to Yale University (P30-EY026878); the NIH to J.A.L. (T32EY22312); and from the NIH to N.M.T. (EY029360).

REFERENCES

Anderson MA, Burda JE, Ren Y, Ao Y, O'Shea TM, Kawaguchi R, Coppola G, Khakh BS, Deming TJ, and Sofroniew MV (2016). Astrocyte scar formation aids central nervous system axon regeneration. Nature 532, 195–200. [PubMed: 27027288]

Bareyre FM, Garzorz N, Lang C, Misgeld T, Büning H, and Kerschen-steiner M (2011). *In vivo* imaging reveals a phase-specific role of STAT3 during central and peripheral nervous system axon regeneration. Proc. Natl. Acad. Sci. USA 108, 6282–6287. [PubMed: 21447717]

Ben-Yaakov K, Dagan SY, Segal-Ruder Y, Shalem O, Vuppalanchi D, Willis DE, Yudin D, Rishal I, Rother F, Bader M, et al. (2012). Axonal transcription factors signal retrogradely in lesioned peripheral nerve. EMBO J. 31, 1350–1363. [PubMed: 22246183]

Berkelaar M, Clarke DB, Wang YC, Bray GM, and Aguayo AJ (1994). Axotomy results in delayed death and apoptosis of retinal ganglion cells in adult rats. J. Neurosci 14, 4368–4374. [PubMed: 8027784]

Bollaerts I, Van Houcke J, Andries L, De Groef L, and Moons L (2017). Neuroinflammation as fuel for axonal regeneration in the injured vertebrate central nervous system. Mediators Inflamm. 2017, 9478542. [PubMed: 28203046]

Bonilla IE, Tanabe K, and Strittmatter SM (2002). Small proline-rich repeat protein 1A is expressed by axotomized neurons and promotes axonal outgrowth. J. Neurosci 22, 1303–1315. [PubMed: 11850458]

Boyd ZS, Kriatchko A, Yang J, Agarwal N, Wax MB, and Patil RV (2003). Interleukin-10 receptor signaling through STAT-3 regulates the apoptosis of retinal ganglion cells in response to stress. Invest. Ophthalmol. Vis. Sci 44, 5206–5211. [PubMed: 14638718]

Bradbury EJ, Moon LD, Popat RJ, King VR, Bennett GS, Patel PN, Fawcett JW, and McMahon SB (2002). Chondroitinase ABC promotes functional recovery after spinal cord injury. Nature 416, 636–640. [PubMed: 11948352]

Bray ER, Yungher BJ, Levay K, Ribeiro M, Dvoryanchikov G, Ayupe AC, Thakor K, Marks V, Randolph M, Danzi MC, et al. (2019). Thrombospondin-1 mediates axon regeneration in retinal ganglion cells. Neuron 103, 642–657.e7. [PubMed: 31255486]

Bregman BS, Kunkel-Bagden E, Schnell L, Dai HN, Gao D, and Schwab ME (1995). Recovery from spinal cord injury mediated by antibodies to neurite growth inhibitors. Nature 378, 498–501. [PubMed: 7477407]

Burmeister AR, and Marriott I (2018). The interleukin-10 family of cytokines and their role in the CNS. Front. Cell. Neurosci 12, 458. [PubMed: 30542269]

Cafferty WB, Yang SH, Duffy PJ, Li S, and Strittmatter SM (2007). Functional axonal regeneration through astrocytic scar genetically modified to digest chondroitin sulfate proteoglycans. J. Neurosci 27, 2176–2185. [PubMed: 17329414]

Cao Z, Gao Y, Bryson JB, Hou J, Chaudhry N, Siddiq M, Martinez J, Spencer T, Carmel J, Hart RB, and Filbin MT (2006). The cytokine inter-leukin-6 is sufficient but not necessary to mimic the peripheral conditioning lesion effect on axonal growth. J. Neurosci 26, 5565–5573. [PubMed: 16707807]

Carvalho LS, Turunen HT, Wassmer SJ, Luna-Velez MV, Xiao R, Bennett J, and Vandenberghe LH (2017). Evaluating efficiencies of dual AAV approaches for retinal targeting. Front. Neurosci 11, 503. [PubMed: 28943836]

Chiou SH, Winters IP, Wang J, Naranjo S, Dudgeon C, Tamburini FB, Brady JJ, Yang D, Grüner BM, Chuang CH, et al. (2015). Pancreatic cancer modeling using retrograde viral vector delivery and *in vivo* CRISPR/Cas9-mediated somatic genome editing. Genes Dev. 29, 1576–1585. [PubMed: 26178787]

Cox LJ, Hengst U, Gurskaya NG, Lukyanov KA, and Jaffrey SR (2008). Intra-axonal translation and retrograde trafficking of CREB promotes neuronal survival. Nat. Cell Biol 10, 149–159. [PubMed: 18193038]

Daya S, and Berns KI (2008). Gene therapy using adeno-associated virus vectors. Clin. Microbiol. Rev 21, 583–593. [PubMed: 18854481]

Dudakov JA, Hanash AM, and van den Brink MR (2015). Interleukin-22: immunobiology and pathology. Annu. Rev. Immunol 33, 747–785. [PubMed: 25706098]

Dupraz S, Grassi D, Karnas D, Nieto Guil AF, Hicks D, and Quiroga S (2013). The insulin-like growth factor 1 receptor is essential for axonal regeneration in adult central nervous system neurons. PLoS ONE 8, e54462. [PubMed: 23349896]

Ertürk A, Mauch CP, Hellal F, Förstner F, Keck T, Becker K, Jährling N, Steffens H, Richter M, Hübener M, et al. (2011). Three-dimensional imaging of the unsectioned adult spinal cord to assess axon regeneration and glial responses after injury. Nat. Med 18, 166–171. [PubMed: 22198277]

Esko JD, Stewart TE, and Taylor WH (1985). Animal cell mutants defective in glycosaminoglycan biosynthesis. Proc. Natl. Acad. Sci. USA 82, 3197–3201. [PubMed: 3858816]

Fischer D, He Z, and Benowitz LI (2004). Counteracting the Nogo receptor enhances optic nerve regeneration if retinal ganglion cells are in an active growth state. J. Neurosci 24, 1646–1651. [PubMed: 14973241]

Fournier AE, GrandPre T, and Strittmatter SM (2001). Identification of a receptor mediating Nogo-66 inhibition of axonal regeneration. Nature 409, 341–346. [PubMed: 11201742]

Glerup S, Kløverpris S, and Oxvig C (2006). The proform of the eosinophil major basic protein binds the cell surface through a site distinct from its C-type lectin ligand-binding region. J. Biol. Chem 281, 31509–31516. [PubMed: 16940047]

GrandPré T, Nakamura F, Vartanian T, and Strittmatter SM (2000). Identification of the Nogo inhibitor of axon regeneration as a Reticulon protein. Nature 403, 439–444. [PubMed: 10667797]

GrandPré T, Li S, and Strittmatter SM (2002). Nogo-66 receptor antagonist peptide promotes axonal regeneration. Nature 417, 547–551. [PubMed: 12037567]

Hammond SL, Leek AN, Richman EH, and Tjalkens RB (2017). Cellular selectivity of AAV serotypes for gene delivery in neurons and astrocytes by neonatal intracerebroventricular injection. PLoS ONE 12, e0188830. [PubMed: 29244806]

Hellström M, and Harvey AR (2011). Retinal ganglion cell gene therapy and visual system repair. Curr. Gene Ther 11, 116–131. [PubMed: 21291357]

Hermens WT, ter Brake O, Dijkhuizen PA, Sonnemans MA, Grimm D, Kleinschmidt JA, and Verhaagen J (1999). Purification of recombinant adeno-associated virus by iodixanol gradient ultracentrifugation allows rapid and reproducible preparation of vector stocks for gene transfer in the nervous system. Hum. Gene Ther 10, 1885–1891. [PubMed: 10446928]

Hernández-Deviez DJ, Roth MG, Casanova JE, and Wilson JM (2004). ARNO and ARF6 regulate axonal elongation and branching through downstream activation of phosphatidylinositol 4-phosphate 5-kinase alpha. Mol. Biol. Cell 15, 111–120. [PubMed: 14565977]

Huebner EA, Kim BG, Duffy PJ, Brown RH, and Strittmatter SM (2011). A multi-domain fragment of Nogo-A protein is a potent inhibitor of cortical axon regeneration via Nogo receptor 1. J. Biol. Chem 286, 18026–18036. [PubMed: 21454605]

Hyatt Sachs H, Schreiber RC, Shoemaker SE, Sabe A, Reed E, and Zigmond RE (2007). Activating transcription factor 3 induction in sympathetic neurons after axotomy: response to decreased neurotrophin availability. Neuroscience 150, 887–897. [PubMed: 18031939]

Ishibashi K, Kanno E, Itoh T, and Fukuda M (2009). Identification and characterization of a novel Tre-2/Bub2/Cdc16 (TBC) protein that possesses Rab3A-GAP activity. Genes Cells 14, 41–52. [PubMed: 19077034]

Jian X, Szaro BG, and Schmidt JT (1996). Myosin light chain kinase: expression in neurons and upregulation during axon regeneration. J. Neurobiol 31, 379–391. [PubMed: 8910795]

Kiu H, and Nicholson SE (2012). Biology and significance of the JAK/STAT signalling pathways. Growth Factors 30, 88–106. [PubMed: 22339650]

Konermann S, Brigham MD, Trevino A, Hsu PD, Heidenreich M, Cong L, Platt RJ, Scott DA, Church GM, and Zhang F (2013). Optical control of mammalian endogenous transcription and epigenetic states. Nature 500, 472–476. [PubMed: 23877069]

Kotenko SV, Izotova LS, Mirochnitchenko OV, Esterova E, Dicken-sheets H, Donnelly RP, and Pestka S (2001). Identification of the functional interleukin-22 (IL-22) receptor complex: the IL-10R2 chain (IL-10Rβ) is a common chain of both the IL-10 and IL-22 (IL-10-related T cell-derived inducible factor, IL-TIF) receptor complexes. J. Biol. Chem 276, 2725–2732. [PubMed: 11035029]

Kragstrup TW, Andersen T, Heftdal LD, Hvid M, Gerwien J, Sivakumar P, Taylor PC, Senolt L, and Deleuran B (2018). The IL-20 cytokine family in rheumatoid arthritis and spondyloarthritis. Front. Immunol 9, 2226. [PubMed: 30319661]

Kwong JM, Quan A, Kyung H, Piri N, and Caprioli J (2011). Quantitative analysis of retinal ganglion cell survival with Rbpms immunolabeling in animal models of optic neuropathies. Invest. Ophthalmol. Vis. Sci 52, 9694–9702. [PubMed: 22110060]

Laaksonen H, Guerreiro-Cacais AO, Adzemovic MZ, Parsa R, Zeitelhofer M, Jagodic M, and Olsson T (2014). The multiple sclerosis risk gene IL22RA2 contributes to a more severe murine autoimmune neuroinflammation. Genes Immun. 15, 457–465. [PubMed: 25008863]

Leaver SG, Cui Q, Plant GW, Arulpragasam A, Hisheh S, Verhaagen J, and Harvey AR (2006). AAV-mediated expression of CNTF promotes long-term survival and regeneration of adult rat retinal ganglion cells. Gene Ther. 13, 1328–1341. [PubMed: 16708079]

Leibinger M, Müller A, Andreadaki A, Hauk TG, Kirsch M, and Fischer D (2009). Neuroprotective and axon growth-promoting effects following inflammatory stimulation on mature retinal ganglion cells in mice depend on ciliary neurotrophic factor and leukemia inhibitory factor. J. Neurosci 29, 14334–14341. [PubMed: 19906980]

Leibinger M, Andreadaki A, Diekmann H, and Fischer D (2013a). Neuronal STAT3 activation is essential for CNTF- and inflammatory stimulation-induced CNS axon regeneration. Cell Death Dis. 4, e805. [PubMed: 24052073]

Leibinger M, Müller A, Gobrecht P, Diekmann H, Andreadaki A, and Fischer D (2013b). Interleukin-6 contributes to CNS axon regeneration upon inflammatory stimulation. Cell Death Dis. 4, e609. [PubMed: 23618907]

Leon S, Yin Y, Nguyen J, Irwin N, and Benowitz LI (2000). Lens injury stimulates axon regeneration in the mature rat optic nerve. J. Neurosci 20, 4615–4626. [PubMed: 10844031]

Li F, Jiang D, and Samuel MA (2019). Microglia in the developing retina. Neural Dev. 14, 12. [PubMed: 31888774]

Liang FQ, Surace E, Dejneka NS, Maguire AM, and Bennett J (2003). Müller cell transduction by AAV2 in normal and degenerative retinas. Adv. Exp. Med. Biol 533, 439–445. [PubMed: 15180296]

Liang SC, Tan XY, Luxenberg DP, Karim R, Dunussi-Joannopoulos K, Collins M, and Fouser LA (2006). Interleukin (IL)-22 and IL-17 are coexpressed by Th17 cells and cooperatively enhance expression of antimicrobial peptides. J. Exp. Med 203, 2271–2279. [PubMed: 16982811]

Ma TC, and Willis DE (2015). What makes a RAG regeneration associated? Front. Mol. Neurosci 8, 43. [PubMed: 26300725]

Macosko EZ, Basu A, Satija R, Nemesh J, Shekhar K, Goldman M, Tirosh I, Bialas AR, Kamitaki N, Martersteck EM, et al. (2015). Highly parallel genome-wide expression profiling of individual cells using nanoliter droplets. Cell 161, 1202–1214. [PubMed: 26000488]

Martin A, Hofmann HD, and Kirsch M (2003). Glial reactivity in ciliary neurotrophic factor-deficient mice after optic nerve lesion. J. Neurosci 23, 5416–5424. [PubMed: 12843240]

Massey JM, Hubscher CH, Wagoner MR, Decker JA, Amps J, Silver J, and Onifer SM (2006). Chondroitinase ABC digestion of the perineuronal net promotes functional collateral sprouting in the cuneate nucleus after cervical spinal cord injury. J. Neurosci 26, 4406–4414. [PubMed: 16624960]

Mattapallil MJ, Kielczewski JL, Zárate-Bladés CR, St Leger AJ, Raychaudhuri K, Silver PB, Jittayasothorn Y, Chan CC, and Caspi RR (2019). Interleukin 22 ameliorates neuropathology and protects from central nervous system autoimmunity. J. Autoimmun 102, 65–76. [PubMed: 31080013]

McKeon RJ, Schreiber RC, Rudge JS, and Silver J (1991). Reduction of neurite outgrowth in a model of glial scarring following CNS injury is correlated with the expression of inhibitory molecules on reactive astrocytes. J. Neurosci 11, 3398–3411. [PubMed: 1719160]

McKerracher L, David S, Jackson DL, Kottis V, Dunn RJ, and Braun PE (1994). Identification of myelin-associated glycoprotein as a major myelin-derived inhibitor of neurite growth. Neuron 13, 805–811. [PubMed: 7524558]

Mehta ST, Luo X, Park KK, Bixby JL, and Lemmon VP (2016). Hyper-activated Stat3 boosts axon regeneration in the CNS. Exp. Neurol 280, 115–120. [PubMed: 27060489]

Müller S, Disse J, Schöttler M, Schön S, Prante C, Brinkmann T, Kuhn J, Kleesiek K, and Götting C (2006). Human xylosyltransferase I and N-terminal truncated forms: functional characterization of the core enzyme. Biochem. J 394, 163–171. [PubMed: 16225459]

Nadal-Nicolás FM, Sobrado-Calvo P, Jiménez-López M, Vidal-Sanz M, and Agudo-Barriuso M (2015). Long-term effect of optic nerve axotomy on the retinal ganglion cell layer. Invest. Ophthalmol. Vis. Sci 56, 6095–6112. [PubMed: 26393669]

Nelson CE, Hakim CH, Ousterout DG, Thakore PI, Moreb EA, Castellanos Rivera RM, Madhavan S, Pan X, Ran FA, Yan WX, et al. (2016). In vivo genome editing improves muscle function in a mouse model of Duchenne muscular dystrophy. Science 351, 403–407. [PubMed: 26721684]

O'Brien JJ, and Nathanson NM (2007). Retrograde activation of STAT3 by leukemia inhibitory factor in sympathetic neurons. J. Neurochem 103, 288–302. [PubMed: 17608645]

Oka Y, Rozek LM, and Czech MP (1985). Direct demonstration of rapid insulin-like growth factor II Receptor internalization and recycling in rat adipocytes: insulin stimulates 125I-insulin-like growth factor II degradation by modulating the IGF-II receptor recycling process. J. Biol. Chem 260, 9435–9442. [PubMed: 2991246]

Overgaard MT, Haaning J, Boldt HB, Olsen IM, Laursen LS, Christiansen M, Gleich GJ, Sottrup-Jensen L, Conover CA, and Oxvig C (2000). Expression of recombinant human pregnancy-associated plasma protein-A and identification of the proform of eosinophil major basic protein as its physiological inhibitor. J. Biol. Chem 275, 31128–31133. [PubMed: 10913121]

Pang JJ, Lauramore A, Deng WT, Li Q, Doyle TJ, Chiodo V, Li J, and Hauswirth WW (2008). Comparative analysis of in vivo and in vitro AAV vector transduction in the neonatal mouse retina: effects of serotype and site of administration. Vision Res. 48, 377–385. [PubMed: 17950399]

Park KK, Liu K, Hu Y, Smith PD, Wang C, Cai B, Xu B, Connolly L, Kramvis I, Sahin M, and He Z (2008). Promoting axon regeneration in the adult CNS by modulation of the PTEN/mTOR pathway. Science 322, 963–966. [PubMed: 18988856]

Pellegrino MJ, and Habecker BA (2013). STAT3 integrates cytokine and neurotrophin signals to promote sympathetic axon regeneration. Mol. Cell. Neurosci 56, 272–282. [PubMed: 23831387]

Perriard G, Mathias A, Enz L, Canales M, Schluep M, Gentner M, Schaeren-Wiemers N, and Du Pasquier RA (2015). Interleukin-22 is increased in multiple sclerosis patients and targets astrocytes.J. Neuroinflammation 12, 119.

Petrs-Silva H, Dinculescu A, Li Q, Min SH, Chiodo V, Pang JJ, Zhong L, Zolotukhin S, Srivastava A, Lewin AS, et al. (2009). High-efficiency transduction of the mouse retina by tyrosine-mutant AAV serotype vectors. Mol Ther. 17, 463–471. [PubMed: 19066593]

Prante C, Bieback K, Funke C, Schön S, Kern S, Kuhn J, Gastens M, Kleesiek K, and Götting C (2006). The formation of extracellular matrix during chondrogenic differentiation of mesenchymal stem cells correlates with increased levels of xylosyltransferase I. Stem Cells 24, 2252–2261. [PubMed: 16778156]

Qiu J, Cafferty WB, McMahon SB, and Thompson SW (2005). Conditioning injury-induced spinal axon regeneration requires signal transducer and activator of transcription 3 activation. J. Neurosci 25, 1645–1653. [PubMed: 15716400]

Rabinovsky ED (2004). The multifunctional role of IGF-1 in peripheral nerve regeneration. Neurol. Res 26, 204–210. [PubMed: 15072640]

Sabat R (2010). IL-10 family of cytokines. Cytokine Growth Factor Rev. 21, 315–324. [PubMed: 21112807]

Santoro F, Mayer D, Klement RM, Warczok KE, Stukalov A, Barlow DP, and Pauler FM (2013). Imprinted Igf2r silencing depends on continuous Airn lncRNA expression and is not restricted to a developmental window. Development 140, 1184–1195. [PubMed: 23444351]

Santos AM, Calvente R, Tassi M, Carrasco MC, Martín-Oliva D, Marín-Teva JL, Navascués J, and Cuadros MA (2008). Embryonic and postnatal development of microglial cells in the mouse retina. J. Comp. Neurol 506, 224–239. [PubMed: 18022954]

Sekine Y, Lin-Moore A, Chenette DM, Wang X, Jiang Z, Cafferty WB, Hammarlund M, and Strittmatter SM (2018). Functional genome-wide screen identifies pathways restricting central nervous system axonal regeneration. Cell Rep. 23, 415–428. [PubMed: 29642001]

Shekhar K, Lapan SW, Whitney IE, Tran NM, Macosko EZ, Kowalczyk M, Adiconis X, Levin JZ, Nemesh J, Goldman M, et al. (2016). Comprehensive classification of retinal bipolar neurons by single-cell transcriptomics. Cell 166, 1308–1323.e30. [PubMed: 27565351]

Shin JE, Cho Y, Beirowski B, Milbrandt J, Cavalli V, and DiAntonio A (2012). Dual leucine zipper kinase is required for retrograde injury signaling and axonal regeneration. Neuron 74, 1015–1022. [PubMed: 22726832]

Silverman SM, and Wong WT (2018). Microglia in the retina: roles in development, maturity, and disease. Annu. Rev. Vis. Sci 4, 45–77. [PubMed: 29852094]

Smith PD, Sun F, Park KK, Cai B, Wang C, Kuwako K, Martinez-Carrasco I, Connolly L, and He Z (2009). SOCS3 deletion promotes optic nerve regeneration in vivo. Neuron 64, 617–623. [PubMed: 20005819]

Smith RP, Lerch-Haner JK, Pardinas JR, Buchser WJ, Bixby JL, and Lemmon VP (2011). Transcriptional profiling of intrinsic PNS factors in the postnatal mouse. Mol. Cell. Neurosci 46, 32–44. [PubMed: 20696251]

Starkey ML, Davies M, Yip PK, Carter LM, Wong DJ, McMahon SB, and Bradbury EJ (2009). Expression of the regeneration-associated protein SPRR1A in primary sensory neurons and spinal cord of the adult mouse following peripheral and central injury. J. Comp. Neurol 513, 51–68. [PubMed: 19107756]

Swiech L, Heidenreich M, Banerjee A, Habib N, Li Y, Trombetta J, Sur M, and Zhang F (2015). In vivo interrogation of gene function in the mammalian brain using CRISPR-Cas9. Nat. Biotechnol 33, 102–106. [PubMed: 25326897]

Tan I, and Leung T (2009). Myosin light chain kinases: division of work in cell migration. Cell Adhes. Migr 3, 256–258.

Templeton JP, and Geisert EE (2012). A practical approach to optic nerve crush in the mouse. Mol. Vis 18, 2147–2152. [PubMed: 22876142]

Toy D, and Namgung U (2013). Role of glial cells in axonal regeneration. Exp. Neurobiol 22, 68–76. [PubMed: 23833555]

Tran NM, Shekhar K, Whitney IE, Jacobi A, Benhar I, Hong G, Yan W, Adiconis X, Arnold ME, Lee JM, et al. (2019). Single-cell profiles of retinal ganglion cells differing in resilience to injury reveal neuroprotective genes. Neuron 104, 1039–1055.e12. [PubMed: 31784286]

Tsujino H, Kondo E, Fukuoka T, Dai Y, Tokunaga A, Miki K, Yonenobu K, Ochi T, and Noguchi K (2000). Activating transcription factor 3 (ATF3) induction by axotomy in sensory and motoneurons: a novel neuronal marker of nerve injury. Mol. Cell. Neurosci 15, 170–182. [PubMed: 10673325]

Wang ZQ, Fung MR, Barlow DP, and Wagner EF (1994). Regulation of embryonic growth and lysosomal targeting by the imprinted Igf2/Mpr gene. Nature 372, 464–467. [PubMed: 7984240]

Wang KC, Koprivica V, Kim JA, Sivasankaran R, Guo Y, Neve RL, and He Z (2002). Oligodendrocyte-myelin glycoprotein is a Nogo receptor ligand that inhibits neurite outgrowth. Nature 417, 941–944. [PubMed: 12068310]

Wang X, Duffy P, McGee AW, Hasan O, Gould G, Tu N, Harel NY, Huang Y, Carson RE, Weinzimmer D, et al. (2011). Recovery from chronic spinal cord contusion after Nogo receptor intervention. Ann. Neurol 70, 805–821. [PubMed: 22162062]

Wang X, Lin J, Arzeno A, Choi JY, Boccio J, Frieden E, Bhargava A, Maynard G, Tsai JC, and Strittmatter SM (2015). Intravitreal delivery of human NgR-Fc decoy protein regenerates axons after optic nerve crush and protects ganglion cells in glaucoma models. Invest. Ophthalmol. Vis. Sci 56, 1357–1366. [PubMed: 25655801]

Wang X, Zhou T, Maynard GD, Terse PS, Cafferty WBJ, Kocsis JD, and Strittmatter SM (2020a). Nogo receptor decoy promotes recovery and corticospinal growth in non-human primate spinal cord injury. Brain 143, 1697–1713. [PubMed: 32375169]

Wang XW, Yang SG, Zhang C, Hu MW, Qian J, Ma JJ, Zhang Y, Yang BB, Weng YL, Ming GL, et al. (2020b). Knocking out non-muscle myosin II in retinal ganglion cells promotes long-distance optic nerve regeneration. Cell Rep. 31, 107537. [PubMed: 32320663]

Watkins TA, Wang B, Huntwork-Rodriguez S, Yang J, Jiang Z, Eastham-Anderson J, Modrusan Z, Kaminker JS, Tessier-Lavigne M, and Lewcock JW (2013). DLK initiates a transcriptional program that couples apoptotic and regenerative responses to axonal injury. Proc. Natl. Acad. Sci. USA 110, 4039–4044. [PubMed: 23431164]

Weinreb RN, Aung T, and Medeiros FA (2014). The pathophysiology and treatment of glaucoma: a review. JAMA 311, 1901–1911. [PubMed: 24825645]

Weyer K, and Glerup S (2011). Placental regulation of peptide hormone and growth factor activity by proMBP. Biol. Reprod 84, 1077–1086. [PubMed: 21270431]

Xie MH, Aggarwal S, Ho WH, Foster J, Zhang Z, Stinson J, Wood WI, Goddard AD, and Gurney AL (2000). Interleukin (IL)-22, a novel human cytokine that signals through the interferon receptor-related proteins CRF2–4 and IL-22R. J. Biol. Chem 275, 31335–31339. [PubMed: 10875937]

Yan W, Laboulaye MA, Tran NM, Whitney IE, Benhar I, and Sanes JR (2020). Mouse retinal cell atlas: molecular identification of over sixty amacrine cell types. J. Neurosci 40, 5177–5195. [PubMed: 32457074]

Yang P, Wen H, Ou S, Cui J, and Fan D (2012). IL-6 promotes regeneration and functional recovery after cortical spinal tract injury by reactivating intrinsic growth program of neurons and enhancing synapse formation. Exp. Neurol 236, 19–27. [PubMed: 22504113]

Yin Y, Cui Q, Li Y, Irwin N, Fischer D, Harvey AR, and Benowitz LI (2003). Macrophage-derived factors stimulate optic nerve regeneration. J. Neurosci 23, 2284–2293. [PubMed: 12657687]

Yungher BJ, Luo X, Salgueiro Y, Blackmore MG, and Park KK (2015). Viral vector-based improvement of optic nerve regeneration: characterization of individual axons' growth patterns and synaptogenesis in a visual target. Gene Ther. 22, 811–821. [PubMed: 26005861]

Zai L, Ferrari C, Dice C, Subbaiah S, Havton LA, Coppola G, Geschwind D, Irwin N, Huebner E, Strittmatter SM, and Benowitz LI (2011). Inosine augments the effects of a Nogo receptor blocker and of environmental enrichment to restore skilled forelimb use after stroke. J. Neurosci 31, 5977–5988. [PubMed: 21508223]

Zenewicz LA, and Flavell RA (2008). IL-22 and inflammation: leukin' through a glass onion. Eur. J. Immunol 38, 3265–3268. [PubMed: 19016525]

Zheng Y, Danilenko DM, Valdez P, Kasman I, Eastham-Anderson J, Wu J, and Ouyang W (2007). Interleukin-22, a T(H)17 cytokine, mediates IL-23-induced dermal inflammation and acanthosis. Nature 445, 648–651. [PubMed: 17187052]

Zhong J (2016). RAS and downstream RAF-MEK and PI3K-AKT signaling in neuronal development, function and dysfunction. Biol. Chem 397, 215–222. [PubMed: 26760308]

Zukor K, Belin S, Wang C, Keelan N, Wang X, and He Z (2013). Short hairpin RNA against PTEN enhances regenerative growth of corticospinal tract axons after spinal cord injury. J. Neurosci 33, 15350–15361. [PubMed: 24068802]

Highlights

- Candidate genes are screened for optic nerve regeneration effects by AAV-shRNA
- Regeneration-limiting genes are confirmed by AAV CRISPR-Cas9 gene editing
- Validated regeneration-limiting genes do not show axotomy-regulated expression
- IL-22 loss activates both Stat3 and DLK, with upregulation of multiple pathways

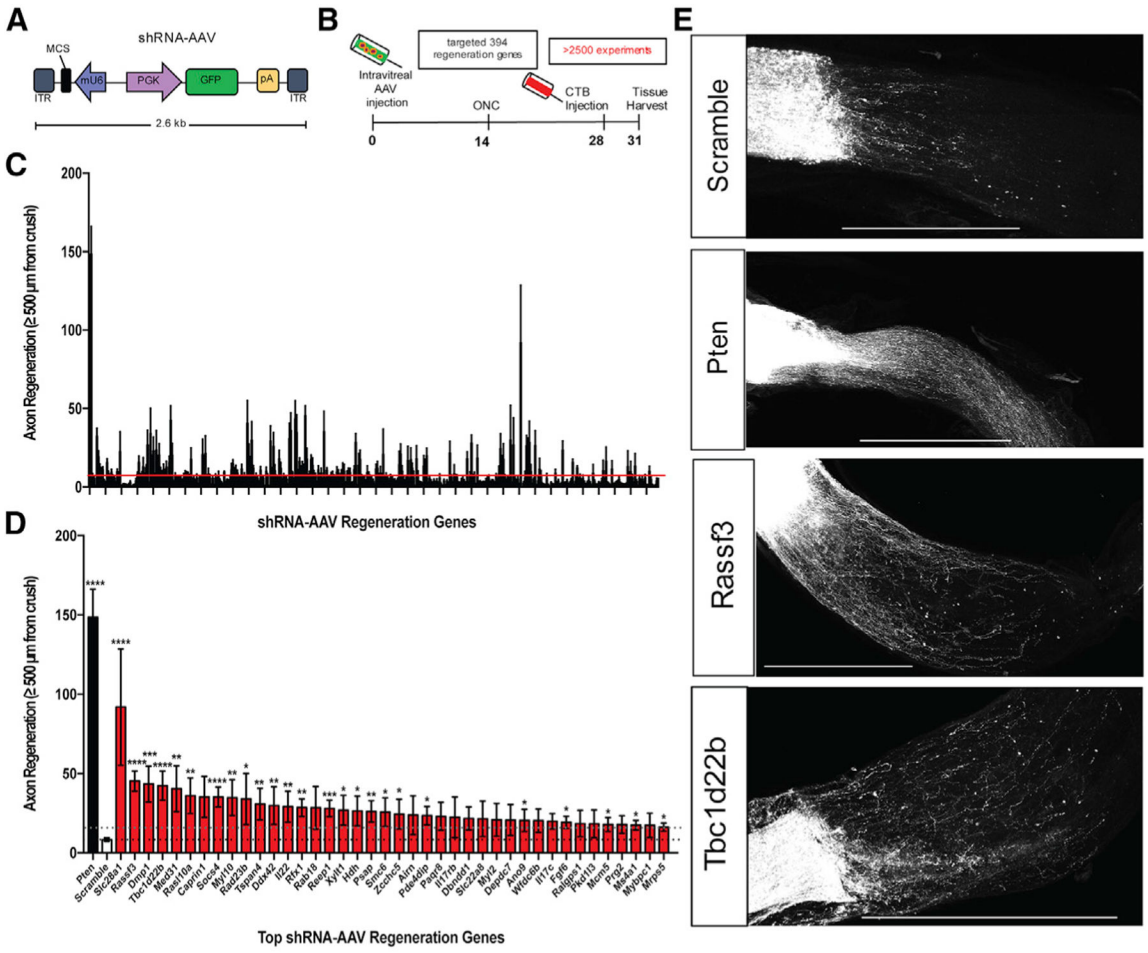

Figure 1. ***In vivo*** **loss-of-function screen reveals functional regeneration genes**

(A and B) Schematic illustration of shRNA-AAV vector for gene-targeted knockdown (A) and AAV injection and ONC injury paradigm (B).

(C) 392 regeneration genes that were identified in a loss-of-function, genome-wide, *in vitro* axon regeneration screen (Sekine et al., 2018) were re-tested *in vivo*.

(D) 40 of the 392 genes showed increased regenerative potential after ONC and were selected for further analysis.

(C and D) Red line in (C) and dotted black line in (D) indicate mean axon regeneration for non-targeted, scramble control. Dotted gray line in (D) indicates scramble mean plus one control standard deviation above the scrambled value. n = 3–10 optic nerves/gene. Data are means ± SEM of axon counts, with one-way ANOVA of natural log (Ln)-transformed values versus scramble. *$p < 0.05$, **$p < 0.01$, ***$p < 0.001$, ****$p < 0.0001$.

(E) Representative confocal z stack maximum-projection images of whole-mount optic nerves 17 d after ONC from scramble, Pten, Rassf3, and Tbc1d22b shRNA-AAV-injected mice. CTB (white) accumulates at the crush site (left) and labels regenerating axons (extending to the right). Scale bars, 500 µm.

See also Figure S1 and Tables S1 and S2.

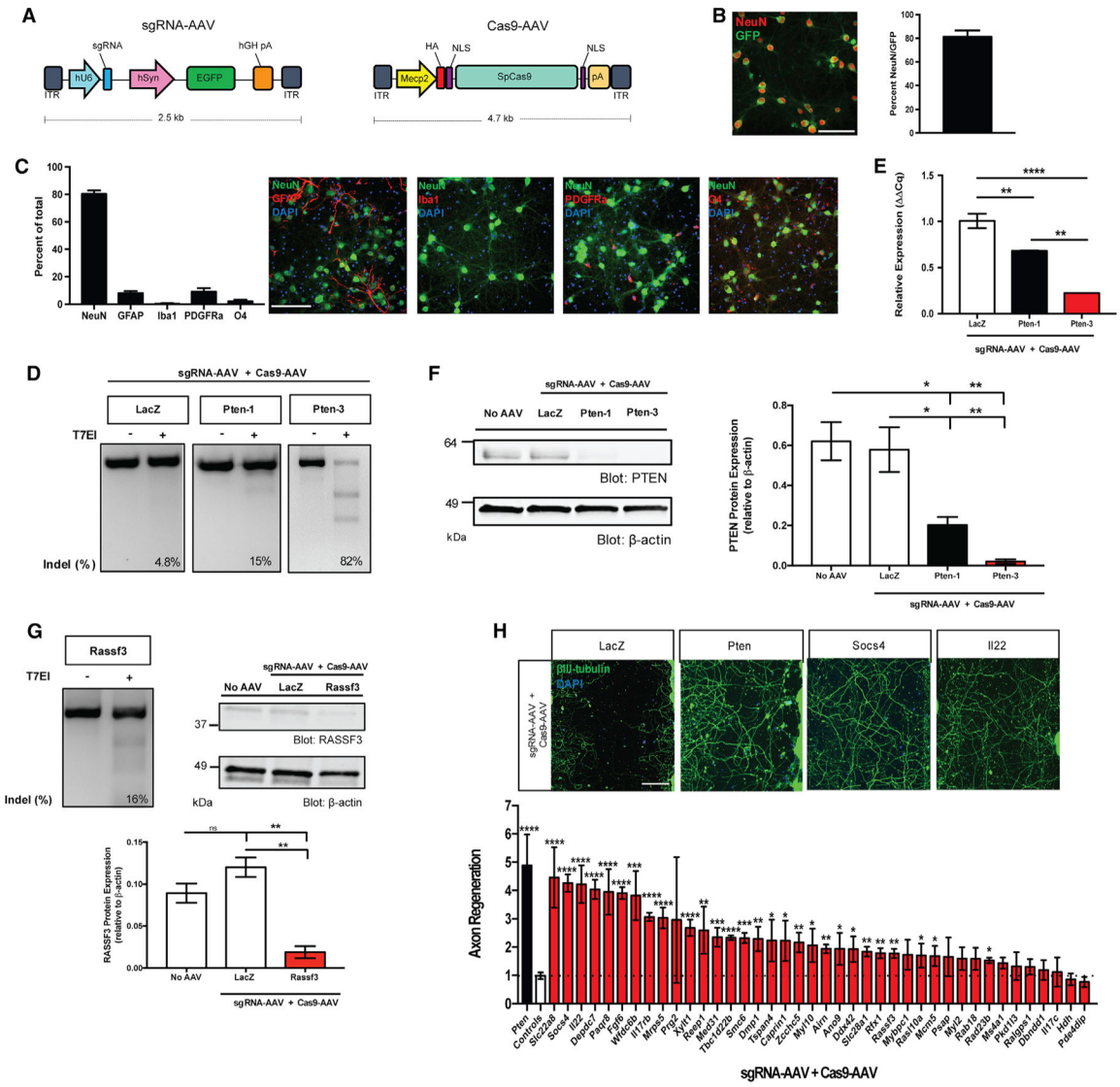

Figure 2. CRISPR-Cas9 gene editing in cortical neurons leads to targeted DNA, RNA, and protein reduction

(A) Schematic illustration of sgRNA-AAV and Cas9-AAV expression vectors. The sgRNA-AAV vector encodes an EGFP sequence for identification of infected retinal cells.

(B) Representative image and quantification of P1 cortical neurons co-transduced with sgRNA-AAV (green) and Cas9-AAV and stained with NeuN (red) to determine neuron-specific infection. Scale bar, 100 μm.

(C) Cellular makeup of untransduced cortical neuron cultures showing quantification and representative images of cultures stained with NeuN (green) and either GFAP (astrocytes), Iba1 (microglia), PDGFRa (oligodendrocyte precursors), or O4 (oligodendrocytes) (red). DAPI (blue) labels cell nuclei. Counts for each cell marker were made in ImageJ and were averaged across 10,350-μm × 350-μm images from different wells. Scale bar, 100 μm.

(D) Evaluation of Pten locus targeting using cortical neurons co-transduced with Cas9-AAV and one of two different sgRNA-AAVs targeting Pten (labeled Pten-1 and Pten-3). sgRNA-AAV targeting LacZ was used as the control and PCR was amplified using Pten-1 primers.

Locus modification efficiencies were analyzed 14 d after transduction with a T7EI endonuclease assay in the presence (+) or absence (−) of the enzyme. Detected indel formation (%) within the Pten locus is indicated.

(E) Relative expression of *Pten* in cortical neurons 14 d after sgRNA-AAV and Cas9-AAV co-transduction was quantified as comparative Ct method (ΔΔCt) normalized to *Gapdh*. n = 3 samples of ~300,000 neurons each. **p < 0.01, ****p < 0.0001, one-way ANOVA with Tukey's test.

(F) Representative immunoblots and quantification of Pten protein reduction in cortical neurons 14 d after sgRNA-AAV and Cas9-AAV co-transduction. Pten expression is normalized to β-actin. n = 3 samples of ~500,000 neurons each. Data are means ± SEM. *p < 0.05, **p < 0.01, one-way ANOVA with Tukey's test. The sgRNA Pten-3 sequence produced the greatest editing efficiency and will hereafter be referred to as "Pten."

(G) Rassf3 DNA and protein-editing efficiency 14 d after sgRNA-AAV transduction. Representative immunoblots with quantification of the Rassf3 protein normalized to β-actin. n = 3 samples of ~500,000 neurons each. **p < 0.01, one-way ANOVA followed by Tukey's test.

(H) Representative images and quantification of axon regeneration for the top 40 genes from the shRNA-AAV *in vivo* screen. Cortical neurons were scraped 14 d after co-transduction with sgRNA-AAV and Cas9-AAV and analyzed 8 d after injury. Neurons transduced with sgRNA-AAVs targeting LacZ, Pten, Socs4, and IL-22 are stained with βIII-tubulin (green) and DAPI (blue). Dotted black line indicates mean axon regeneration for non-targeted LacZ control. n = 3 experiments of ~500,000 neurons/gene/experiment, Student's t test versus controls, in which controls are the combined average values of LacZ, Cas9-AAV only (i.e., no sgRNA-AAV), and naive/untransduced cortical neurons. Data are means ± SEM. *p < 0.05, **p < 0.01, ***p < 0.001, ****p < 0.0001. Scale bar, 100 μm.

See also Tables S2–S4.

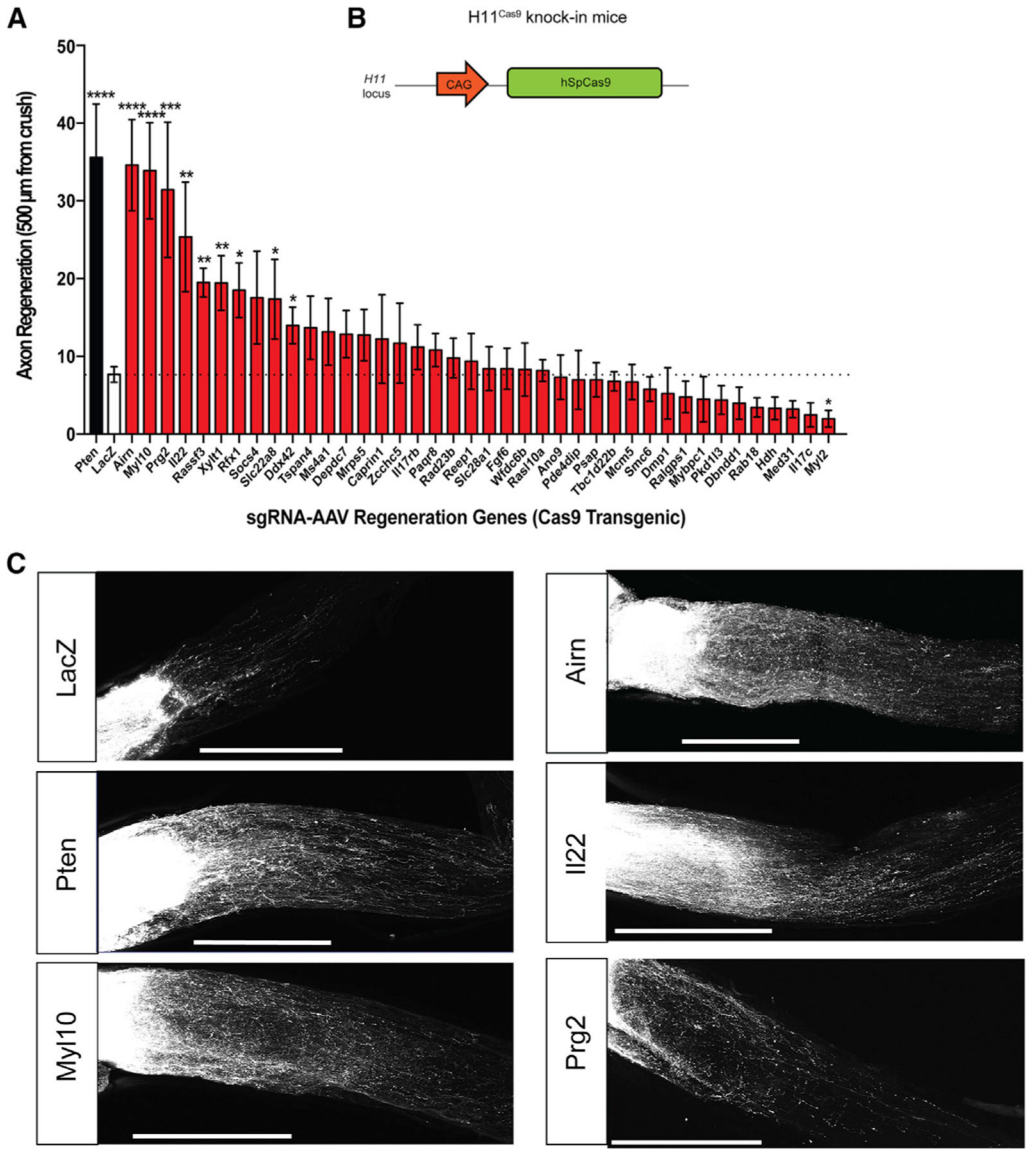

Figure 3. ***In vivo*** **optic nerve regeneration analysis using the CRISPR-Cas9**

(A) Axon regeneration using Cas9 transgenic mice and sgRNA-AAV targeting the 40 genes identified in Figure 1. Dotted black line is mean axon regeneration for non-targeted LacZ control. n = 3–10 nerves/gene. Data are means ± SEM of axon counts, with one-way ANOVA of Ln-transformed values versus the LacZ control. *p < 0.05, **p <0.01, ***p < 0.001, ****p < 0.0001.

(B) Schematic of $H11^{Cas9}$ CRISPR-Cas9 knock-in mice.

(C) Representative confocal maximum projection images of whole-mount optic nerves 17 d after ONC from LacZ, Pten, Myl10, Airn, IL-22, and Prg2 sgRNA-AAV-injected mice. CTB (white) accumulates at the crush site (left) and labels regenerating axons (extending to the right). Scale bars, 500 µm.

See also Figures S1 and S2 and Tables S2 and S3.

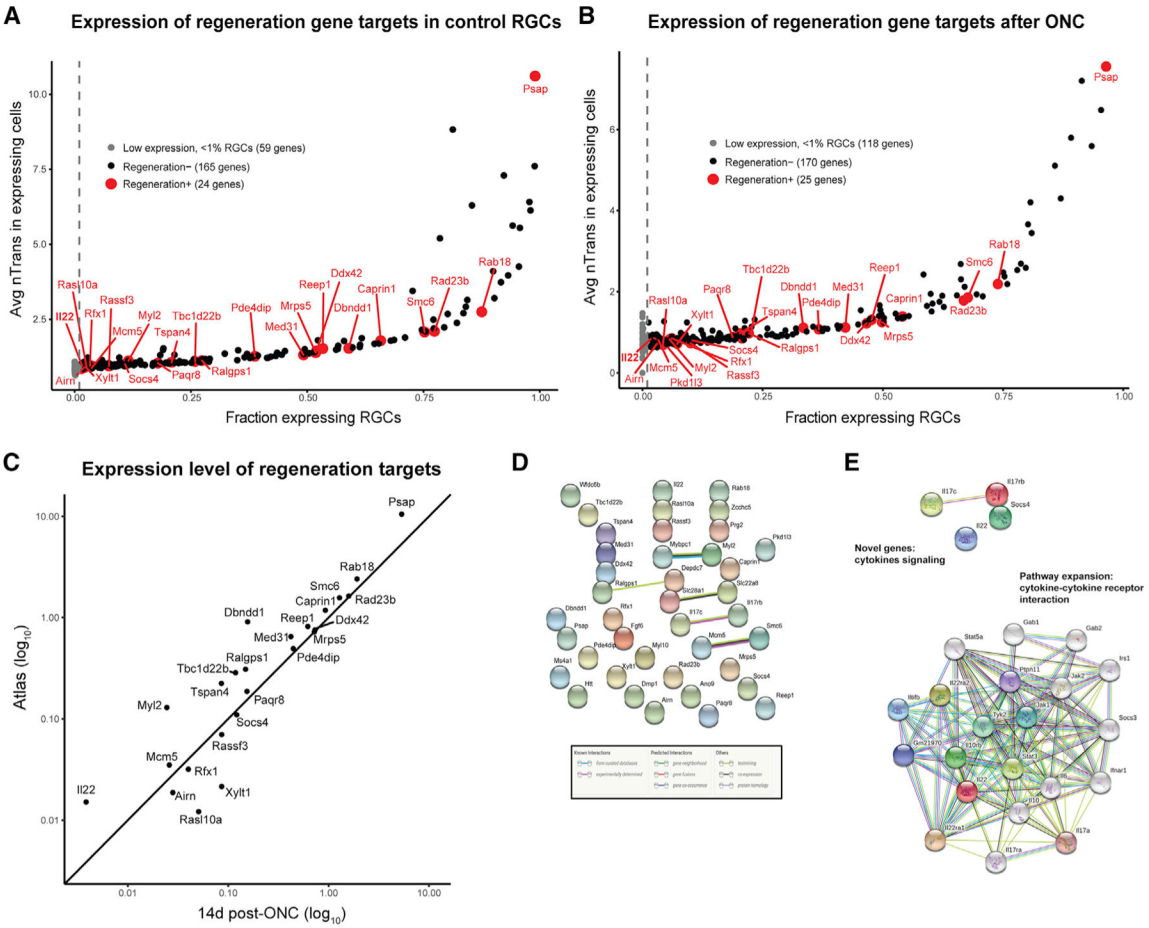

Figure 4. Regeneration genes are largely not regulated by axotomy and participate in multiple pathways

(A) Scatterplot showing expression of regeneration gene targets (average number of transcripts in expressing cells) and total fraction of RGCs with detected transcripts in control RGCs. The dotted gray line is drawn at 0.01 and demarcates a threshold for genes expressed in 1% of cells (below threshold targets are colored gray dots). Twenty-four of the 40 positive regeneration genes (red dots) are expressed in >1% of RGCs. Black dots indicate genes expressed in >1% of RGCs that were designated as having a lesser regeneration phenotype after ONC.

(B) Scatterplot showing average expression of regeneration gene targets and fraction expressing cells in injured RGCs (merged data from 0.5, 1, 2, 4, 7, and 14 d after ONC).

(C) Expression levels before and 14 d after ONC of the 24 positive regeneration genes expressed in >1% of RGCs. The overall average expression level is calculated as (average number of transcripts in expressing cells) × (total fraction of RGCs with detected transcripts). “Atlas” data are the average expression level from 35,699 P56 mouse RGCs pooled across types.

(D) The interaction network for the list of regeneration genes constructed using STRING database. Known and predicted interactions, as well as co-expression and text-mining, are shown by connecting lines.

(E) Expansion of the interaction network for genes with cytokine signaling function (IL-22, IL-17c, IL-17rb, and Socs4) identifies Stat3 as a binding partner for IL-22, one of the top regeneration genes identified in Figures 1, 2, and 3.
See also Figures S3 and S4 and Tables S5, S6, and S7.

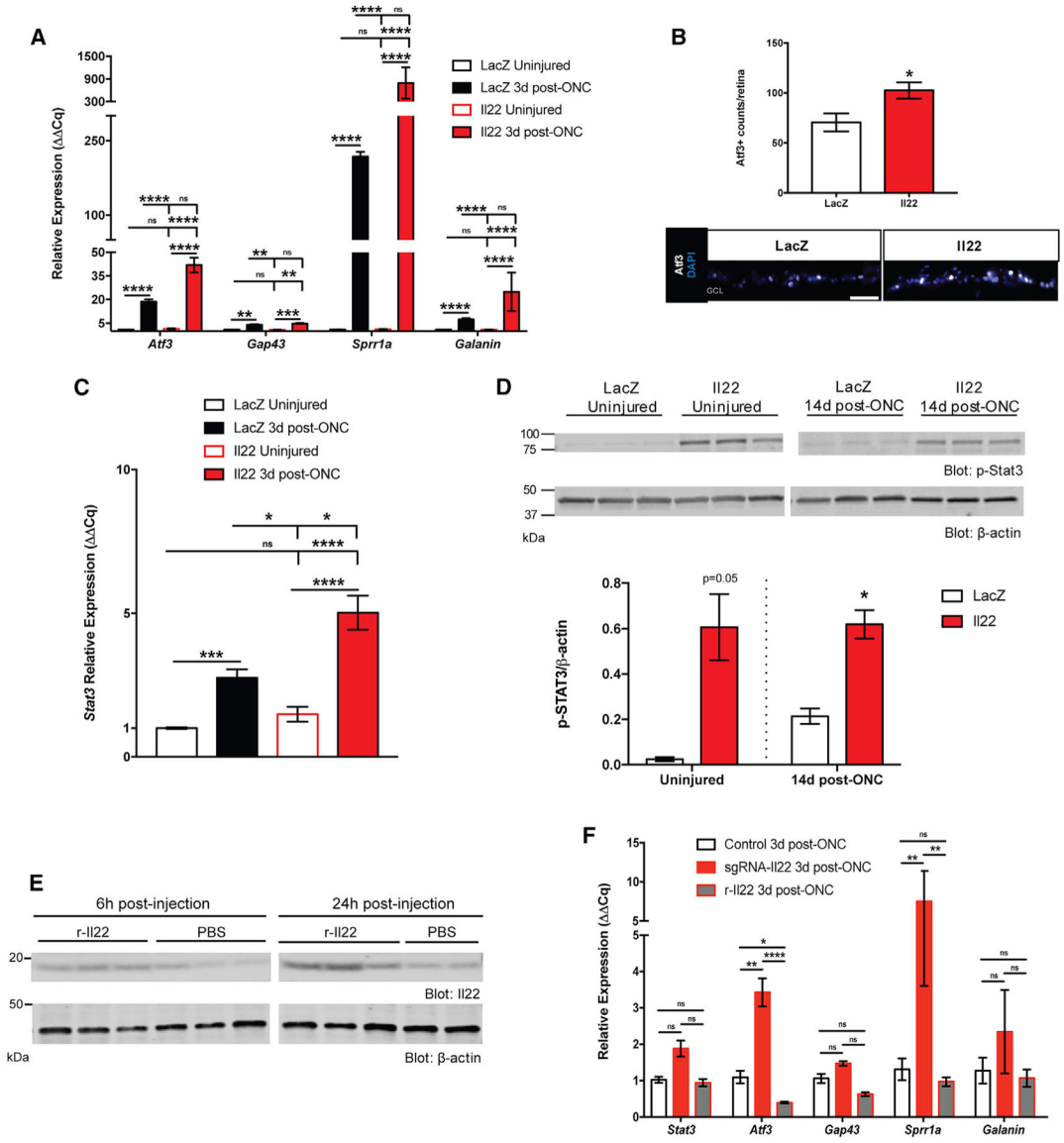

Figure 5. Reduction of IL-22 drives a pro-regenerative RAG and Stat3 expression program in the retina after injury

(A) Relative mRNA expression of RAGs in the retina after LacZ or IL-22-targeted sgRNA-AAV infection and 3 d after ONC was quantified using the ΔΔCt method normalized to the housekeeping gene *Gapdh*. n = 4 retinas/group/time. Data are means ± SEM of comparative quantification (ΔΔCq), with one-way ANOVA of Ln-transformed values and Tukey's test. **p < 0.01, ***p < 0.001, ****p < 0.0001.

(B) Quantification and representative images of Atf3 immunostaining in LacZ- or IL-22-sgRNA-targeted retinas 3 d after injury. n = 5 retinas/group. Data are means ± SEM. **p < 0.01, Student's t test. Scale bar, 50 μm. GCL, ganglion cell layer. A threshold fluorescence was used to count $Atf3^{+}$ cells. Counts are from four separate retina cross-sections from each animal. The GCL was identified by DAPI, and counts were normalized to the layer area.

(C) Relative *Stat3* mRNA expression inretina after LacZ- or IL-22-targeted sgRNA-AAV infection and 3 d after ONC was quantified using ΔΔCt normalized to *Gapdh*. n = 4 retinas/

group/time. Data are means ± SEM of ΔΔCq, with one-way ANOVA of Ln-transformed values and Tukey's test. *p < 0.05, ***p < 0.001, ****p < 0.0001.

(D) Retinal p-Stat3 protein expression was quantified 14 d after ONC. IL-22 editing with injury significantly increases p-Stat3 protein levels compared with the LacZ control. n = 3 retinas/group/time. Data are means ± SEM. *p < 0.05, Student's t test within uninjured or injured groups because experiments were performed separately.

(E) Intravitreal delivery of r-IL-22 increased IL-22 protein in the retina 1 d after injection.

(F) PBS or r-IL-22 was injected into the vitreous cavity of WT mice 1 d before ONC. Retinas were isolated 3 d after injury for qPCR. Relative mRNA expression in the retina 3 d after ONC was quantified as ΔΔCt normalized to *Gapdh* and compared with controls, the average values of injured LacZ-AAV and PBS retinas. n = 4 retinas/group/time. Data are means ± SEM of ΔΔCq, with one-way ANOVA of Ln-transformed values and Tukey's test. *p < 0.05, **p < 0.01, ****p < 0.0001. sgRNA LacZ and IL-22 qPCR raw data from (A) were used for analysis.

See also Figure S5 and Table S4.

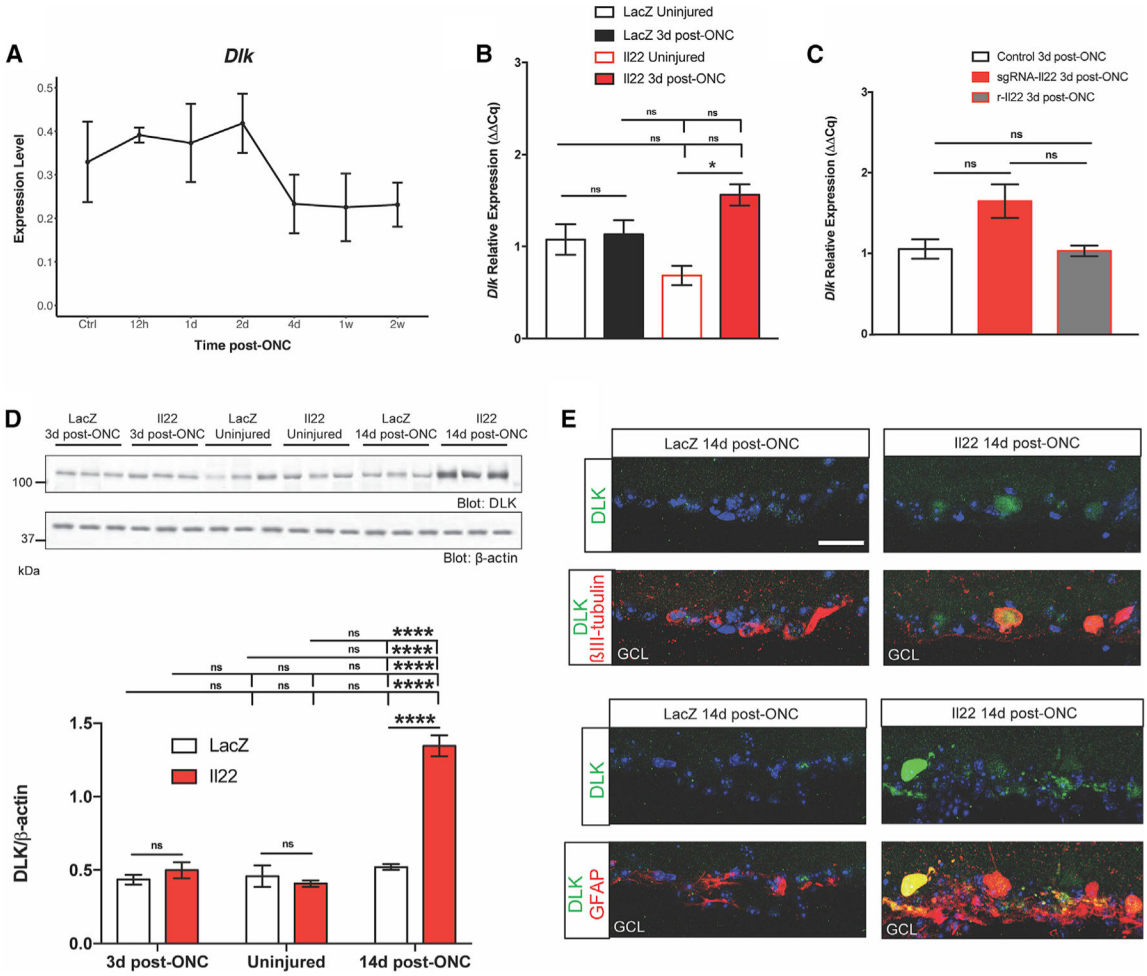

Figure 6. Inhibition of IL-22 enhances DLK expression in the retina after ONC

(A) Average expression level of *Dlk* in adult mouse RGCs by scRNA-seq before and at six time points (0.5–14 d) after ONC (replotted from dataset described in Tran et al., 2019). Means with SD for biological replicates (3–5 per time). Expression is defined as (average number of transcripts in expressing cells) × (fraction of expressing RGCs).

(B) Relative expression of *Dlk* in the retina after LacZ- or IL-22-targeted sgRNA-AAV infection and 3 d after ONC was quantified as ΔΔCt normalized to *Gapdh*. n = 8 retinas/group/time. Data are means ± SEM of ΔΔCq, with one-way ANOVA of Ln-transformed values and Tukey's test. *p < 0.05.

(C) Relative mRNA expression of *Dlk* in the retina 3 d post-ONC after PBS or r-IL-22 injection was quantified as ΔΔCt normalized to the housekeeping gene *Gapdh* and compared with controls, which were the combined average Ct values of injured LacZ-AAV and PBS retinas. n = 4 retinas/group/time. Data are means ± SEM of ΔΔCq, with one-way ANOVA of Ln-transformed values and Tukey's test.

(D) Retinal DLK protein expression was quantified at 3 and 14 d after ONC. Immunoblots and quantification indicate that IL-22 editing significantly enhances DLK protein levels. n = 6 retinas/group/time. Data were from two blots, in which each blot had n = 3 per group/time. Data are means ± SEM. ****p < 0.0001, one-way ANOVA and Tukey's test.

(E) Representative images of DLK (green) and either βIII-tubulin or GFAP (red) in the unedited or IL-22-edited retina 14 d after ONC. Scale bar, 20 μm. Nuclei are stained with DAPI (blue).

See also Figure S5 and Table S4.

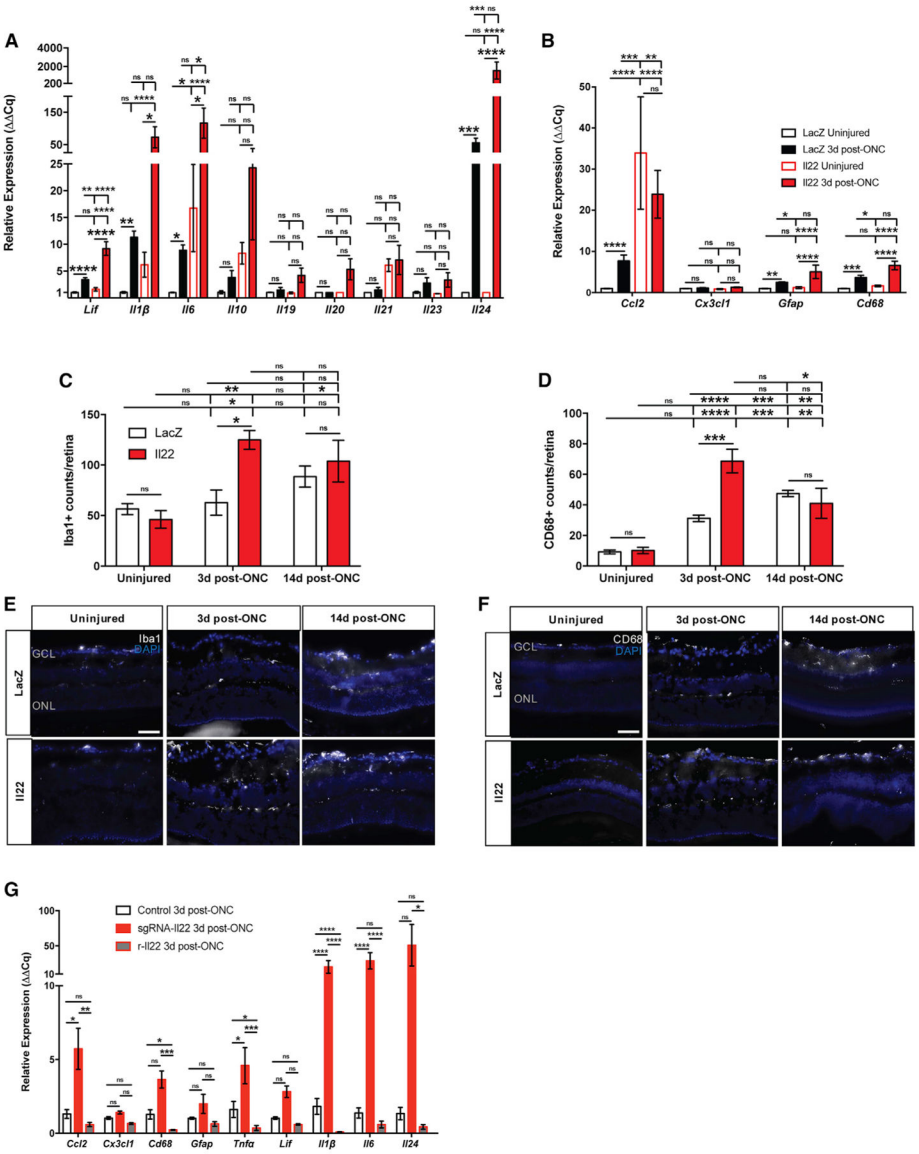

Figure 7. IL-22 editing stimulates the transcriptional expression of numerous genes implicated in axon regeneration and increases microglia/macrophage transcripts and cell accumulation in the retina

(A and B) Relative mRNA expression of inflammatory cytokine (A) and glial cell (B) activators in the retina after LacZ- or IL-22-targeted sgRNA-AAV infection and 3 d after ONC was quantified as ΔΔCt normalized to *Gapdh*. n = 4 retinas/group/time. Data are means ± SEM of ΔΔCq, with one-way ANOVA of Ln-transformed values and Tukey's test. *p < 0.05, **p < 0.01, ***p < 0.001, ****p < 0.0001.

(C and E) Quantification (C) and representative images (E) of Iba1^{+} microglia/macrophages in the unedited or edited retina 3 and 14 d after ONC are represented as the total number of Iba1^{+} cells counted in four separate images of retinal cross-sections from the same animal. Retinal layers were identified by DAPI, and counts were normalized to the layer area. n = 5 retinas/group/time. Data are means ± SEM. *p < 0.05, **p < 0.01, one-way ANOVA and Tukey's test. Scale bar, 50 μm.

(D and F) Quantification (D) and representative images (F) of $CD68^+$ microglia/macrophages in the unedited or edited retina 3 and 14 d after ONC are the total number of $CD68^+$ cells counted in four separate images of retinal tissue from the same animal. n = 5 retinas/group/time. Data are means ± SEM. *p < 0.05, **p <0.01, ***p < 0.001, ****p < 0.0001, one-way ANOVA and Tukey's test. Scale bar, 50 μm. Nuclei stained with DAPI (blue).

(G) PBS or r-IL-22 were injected into the vitreous cavity of WT mice 1 d before ONC. Retinas were isolated 3 d after injury for qPCR. Relative mRNA expression of indicated genes in the retina 3 d after ONC was quantified as ΔΔCt), normalized to *Gapdh* and compared with controls, from injured LacZ-AAV and PBS retinas. n = 4 retinas/group/time. Data are means ± SEM of ΔΔCq, with one-way ANOVA of Ln-transformed values and Tukey's test. *p < 0.05, **p < 0.01, ***p < 0.001, ****p < 0.0001. sgRNA LacZ and IL-22 qPCR data from (A) and (B) were used for analysis.

See also Figures S6 and S7 and Table S4.

KEY RESOURCES TABLE

REAGENT or RESOURCE	SOURCE	IDENTIFIER
Antibodies		
Anti-Rbpms	PhosphoSolutions	Cat#1830-Rbpms; RRID:AB_2492225
Anti-Rbpms	PhosphoSolutions	Cat#1832-Rbpms; RRID:AB_2492226
Anti-Rbpms	Proteintech	Cat#15187-1-AP; RRID:AB_2238431
Anti-Brn3a	Abcam	Cat#ab81213; RRID:AB_1640222
Anti-NeuN	Millipore	Cat#ABN91; RRID:AB_11205760
Anti-GFAP	Dako	Cat#Z0334; RRID:AB_10013382
Anti-Iba1	Wako	Cat#019-19741; RRID:AB_839504
Anti-PDGF Receptor a	CST	Cat#3174; RRID:AB_2162345
Anti-O4	R&D Systems	Cat#MAB1326; RRID:AB_357617
Anti-βIII-tubulin	Promega	Cat#G712A; RRID:AB_430874
Anti-Pten	CST	Cat#9559; RRID:AB_390810
Anti-Il22	Millipore	Cat#AV49523; RRID:AB_1851697
Anti-p-STAT3	CST	Cat#9145; RRID:AB_2491009
Anti-DLK	Genetex	Cat#GTX124127; RRID:AB_11170703
Anti-β-actin	CST	Cat#3700; RRID:AB_2242334
Anti-β-actin	CST	Cat#4967; RRID:AB_330288
Anti-Iba1	Abcam	Cat#ab178846; RRID:AB_2636859
Anti-CD68	Bio-Rad	Cat#MCA1957; RRID:AB_322219
Anti-GFAP	Abcam	Cat#ab7260; RRID:AB_305808
Anti-GFAP	Abcam	Cat#ab53554; RRID:AB_880202
Anti-GFP	Abcam	Cat#ab13970; RRID:AB_300798
Anti-Il22Ra1	Bioss	Cat#bs-2624R; RRID:AB_10857827
Anti-Atf3	Novus Biologicals	Cat#NBP1-85816; RRID:AB_11014863
Anti-CD16/CD32	Biolegend	Cat#101302; RRID:AB_312801
Alexa Fluor 546	Invitrogen	Cat#A11035; RRID:AB_2534093
Alexa Fluor 594	Thermo Fisher	Cat#A-11058; RRID:AB_2534105
Alexa Fluor 647	Invitrogen	Cat#A21245; RRID:AB_2535813
Alexa Fluor 647	Invitrogen	Cat#A31573; RRID:AB_2536183
Alexa Fluor 647	Invitrogen	Cat#A31571; RRID:AB_162542
Alexa Fluor 647	Invitrogen	Cat#A21247; RRID:AB_141778
Alexa Fluor 647	Thermo Fisher	Cat#A-21450; RRID:AB_2735091
Alexa Fluor 488	Invitrogen	Cat#A11034; RRID:AB_2576217
Alexa Fluor 488	Invitrogen	Cat#A11073; RRID:AB_2534117
Alexa Fluor 488	Invitrogen	Cat#A11039; RRID:AB_2534096
Alexa Fluor 488	Invitrogen	Cat#SA1-72000; RRID:AB_923386
Alexa Fluor 488	Thermo Fisher	Cat#A21042; RRID:AB_2535711
Alexa Fluor 555	Thermo Fisher	Cat#A31572; RRID:AB_162543
APC	R&D Systems	Cat#F0111; RRID:AB_573127
IRDye 680	Li-Cor	Cat#926-68072; RRID:AB_10953628

REAGENT or RESOURCE	SOURCE	IDENTIFIER
IRDye 680	Li-Cor	Cat#926-68073; RRID:AB_10954442
IRDye 800	Li-Cor	Cat#926-32213; RRID:AB_621848
IRDye 800	Li-Cor	Cat#926-32212; RRID:AB_621847
Bacterial and virus strains		
One Shot Stbl3 Chemically Competent *E. coli*	Thermo Fisher	Cat#737303
Chemicals, peptides, and recombinant proteins		
FBS	GIBCO	Cat##10437028
DMEM	GIBCO	Cat#11965-092
Hibernate-E	BrainBits	Cat#HE-Ca
Neurobasal-A	GIBCO	Cat#10888022
GlutaMAX	GIBCO	Cat#35050-061
B-27	GIBCO	Cat#17504044
Penicillin/streptomycin	GIBCO	Cat#15140-122
Papain	Worthington Biochemical	Cat #LS003127
DnaseI	Sigma-Aldrich	Cat#DN-25
Benzonase nuclease	Millipore	Cat#70746-10KUN
T4 DNA Ligase	NEB	Cat#M0202
T7 DNA Ligase	NEB	Cat#M0318
EcoR I	NEB	Cat# R0101
BamH I	NEB	Cat#R0136
Sap I	Thermo Fisher	Cat#FD1934
Polyethylenimine	Polysciences, Inc.	Cat##23966-1
iQ SYBR Green Supermix	Bio-Rad	Cat#1708882
DAPI	Bio-Rad	Cat#135-1303
QuickExtract DNA Extraction Solution	Lucigen	Cat##QE09050
Cholera Toxin Subunit B Alexa Fluor 555 Conjugate	Thermo Fisher	Cat#C34766
Recombinant Murine IL-22	Peprotech	Cat#210-22
Critical commercial assays		
Alt-R Genome Editing Detection Kit	IDT	Cat#1075932
Mouse/Rat Il-22 Quantikine ELISA kit	R&D Systems	Cat#M2200
RNeasy Plus Mini Kit	QIAGEN	Cat#74134
iScript cDNA Synthesis Kit	Bio-Rad	Cat#1708891
Taqman Gene Expression Master Mix	Applied Biosystems	Cat#4369016
DNeasy Blood and Tissue Kit	QIAGEN	Cat#69504
Experimental models: cell lines		
HEK293T	ATCC	Cat#CRL-3216
Experimental models: organisms/strains		
C57BL/6J		The Jackson Laboratory Cat#000664
$H11^{Cas9}$	Chiou et al., 2015	The Jackson Laboratory Cat#027650
Oligonucleotides		
See Table S1 for shRNA list		N/A

REAGENT or RESOURCE	SOURCE	IDENTIFIER
See Table S3 for sgRNA list		N/A
See Table S4 for qPCR primer list		N/A
Recombinant DNA		
pAAV-U6-GFP Expression Vector	Cell Biolabs	Cat#VPK-413
PX551	Swiech et al., 2015	Addgene Plasmid #60957
PX552	Swiech et al., 2015	Addgene Plasmid #60958
Software and algorithms		
Prism 7.04	GraphPad	https://www.graphpad.com
ImageJ	NIH	https://imagej.nih.gov/ij/
String	bioinformatical analysis	https://string-dborg/